Nonlinear Dynamics (2026) 114:1089
https://doi.org/10.1007/s11071-026-12948-0

RESEARCH

Basins of attraction and dynamic integrity in 1-DOF autonomous systems with quadratic drag

Attila Genda[1] · Alexander Fidlin[1] · Oleg V. Gendelman[2]

Received: 3 February 2026 / Revised: 2 July 2026 / Accepted: 4 August 2026

Abstract
Quadratic air drag is a standard dissipative mechanism in mechanical models, particularly when velocities are not small. In nonlinear systems, where multiple attractors may co-exist, analytical solutions for the motion are rarely available. For conservative one-degree-of-freedom systems, conservation of energy can be used to determine separatrices that divide phase space into regions with qualitatively different dynamics, such as bounded and unbounded motion. However, in the presence of damping, energy conservation no longer holds, and analytical descriptions of basin-of-attraction boundaries remain scarce. This paper studies autonomous one-degree-of-freedom systems with air drag of the form

$$\ddot{x} + \alpha(x)|\dot{x}|\dot{x} + V'(x) = 0,$$

and targets the constructive determination of the *basins of attraction* and the associated basin boundaries in the $(x, \dot{x})$ plane. On trajectory segments with fixed velocity sign, the substitution $p(x) = \dot{x}^2$ converts the second-order dynamics into a first-order linear equation for p as a function of x. For the polynomial potentials considered here, this reduction yields explicit integral representations and, in several cases, closed-form expressions that can be continued branchwise from the saddle to generate separatrix-type curves in phase space. These curves provide exact boundaries that partition initial conditions either into different capture regimes or into capture versus escape, depending on the potential under investigation. In addition, the local integrity measures associated with the attractors are obtained analytically. Analytical results are verified against direct time-domain simulations. The resulting closed-form formulas provide benchmark cases for validating numerical algorithms that aim to determine dynamic integrity measures.

Keywords Quadratic air drag · Quadratic damping · Basin of attraction · Basin boundary · Separatrix · Turning point · Bistable Duffing oscillator · Quadratic-cubic potential

Mathematics Subject Classification 34C15 · 34A34 · 37C29 · 37N15 · 70K44

✉ Attila Genda
attila.genda@kit.edu

Alexander Fidlin
alexander.fidlin@kit.edu

Oleg V. Gendelman
ovgend@technion.ac.il

1 Institute of Engineering Mechanics, Karlsruhe Institute of Technology, Karlsruhe, Germany

2 Mechanical Engineering, Technion – Israel Institute of Technology, Haifa, Israel

1 Introduction

Aerodynamic drag is an essential component of realistic mechanical models whenever motion occurs in a fluid. In many practically relevant regimes, the dissipative force is well approximated by a quadratic law in the velocity magnitude. This motivates the widespread use of quadratic damping in applications such as ship roll dynamics and related marine models [1–5], as well as in pendulum experiments and large-angle oscillations [6, 7]. Beyond these classical examples, quadratic drag is routinely employed in wave loading and response models for offshore and coastal structures via Morison-type formulations [8, 9], in the dynamics of underwater vehicles and towed bodies [10], in central-force motion models [11], and in the modeling of strongly speed-dependent dissipation in parachutes and other bluff-body problems [12, 13]. Quadratic drag models are also standard in sports-ball and projectile flight modeling [14–16]. Even when the primary interest is not fluid mechanics itself, quadratic drag often provides the simplest dissipative closure that fits observed decay and captures the strong increase of energy loss with speed.

We study the one-degree-of-freedom motion in a potential well with quadratic drag:

$$\ddot{x} + \alpha(x)\,|\dot{x}|\,\dot{x} + V'(x) = 0, \qquad \alpha(x) \geq 0, \tag{1}$$

interpreted branchwise in the phase plane so that the dissipative term opposes the motion. The coefficient $\alpha(x)$ may represent variations in effective drag with position (e.g., due to geometry, density, or projected area). The key simplification for autonomous 1-DOF systems is obtained by introducing the squared velocity $p(x) = \dot{x}^2$ on any branch with fixed velocity sign $\sigma = \operatorname{sgn}(\dot{x})$. This transforms (1) into a first-order equation for p as a function of x that is linear on each branch after accounting for σ, which enables explicit integral representations and, for many potentials, closed-form expressions. This energy-displacement viewpoint goes back to classical vibration theory and has been used repeatedly to describe decay per cycle and turning-point sequences [17–20], supported by standard asymptotic frameworks [21–23] and by later exact and semi-exact treatments for broad restoring force classes [24–26]. Related modern analytic research includes integrability conditions and solvable potentials under quadratic drag [27–29]. Quadratic drag entered analytical mechanics prominently through exterior ballistics. Therefore, we also recall the classical and historical projectile literature, from Newton's resisting-medium model and Bernoulli's hodograph treatment to later ballistic approximations and reviews [30–39], as well as modern non-elementary or semi-analytical representations of projectile motion with quadratic resistance [40–43]. However, planar projectile motion is used here only as a physical motivation for quadratic drag, not as a target application of the present basin-boundary framework: the classical projectile problem is a two-degree-of-freedom flight problem without the saddle-type equilibria that generate the basin boundaries studied below.

Despite the extensive literature on quadratic drag, most works focus on decay envelopes, frequency shifts, the identification of damping laws, forced response, or projectile trajectories. The present study focuses on a different output: *basins of attraction* and *escape thresholds*. Concretely, the goal is to obtain explicit separatrix-type curves in the $(x, \dot{x})$ plane that partition initial conditions into capture and escape. Adjacent literature does address escape and basin geometry under dissipation, but typically in forced oscillators or in multi-degree-of-freedom settings [44, 45], or they provide existence and classification results without explicit basin-of-attraction boundaries for prescribed potentials [46]. This leaves a gap for explicit phase-plane partitions in autonomous potentials with quadratic drag.

The present paper is the first part of a planned trilogy. Accordingly, the series delivers explicit basin boundaries in the phase plane for representative nonlinear potentials with quadratic drag. These curves provide direct threshold conditions for separating long-time outcomes (capture in a given well, barrier crossing, or escape, where admissible) and are verified against time-domain simulations.

Such analytically parameterized basin boundaries are also helpful as benchmark test cases for *dynamical integrity* methods, where robustness is quantified from the geometry of safe basins [47–50]. Since integrity measures are typically estimated from grids or sample-based strategies [51], closed or semi-closed basin boundaries offer rare ground truth for assessing computational procedures, including recent efficient integrity algorithms for equilibria and periodic orbits [52, 53] and forced-escape integrity studies [54].

The paper is structured as follows. Section 2 derives the branchwise substitution $p(x) = \dot{x}^2$ and the turning-point and branch-switching rules. Section 3 applies the method to the quadratic-cubic potential. Section 4 treats the bistable Duffing potential. Section 5 analyzes the quadratic-quartic potential with two barriers. Section 6 summarizes the main findings and discusses parameter-dependent bifurcations. Section 7 outlines future extensions.

2 Branchwise reduction to a first-order linear ODE

A central simplification for the autonomous 1-DOF model (1) is obtained by using the squared velocity as an unknown function of position,

$$p(x) := \dot{x}^2 \geq 0, \tag{2}$$

defined along trajectory segments on which $\dot{x} \neq 0$. On such a segment, the velocity sign

$$\sigma := \operatorname{sgn}(\dot{x}) \in \{+1, -1\} \tag{3}$$

is constant, and the quadratic and Coulomb terms can be written as $|\dot{x}|\dot{x} = \sigma\, p$ and $\operatorname{sgn}(\dot{x}) = \sigma$, respectively. Moreover, since

$$\frac{\mathrm{d}p}{\mathrm{d}t} = 2\dot{x}\,\ddot{x}, \qquad \frac{\mathrm{d}p}{\mathrm{d}x} = \frac{\mathrm{d}p/\mathrm{d}t}{\mathrm{d}x/\mathrm{d}t} = \frac{2\dot{x}\,\ddot{x}}{\dot{x}} = 2\ddot{x} \quad (\dot{x} \neq 0), \tag{4}$$

the equation of motion reduces on each fixed-σ branch to the linear first-order equation

$$\frac{\mathrm{d}p}{\mathrm{d}x} + 2\sigma\,\alpha(x)\,p = -2V'(x). \tag{5}$$

Thus, for prescribed functions $\alpha(x)$, and $V(x)$, the dynamics are determined by solving (5) separately for $\sigma = +1$ and $\sigma = -1$, and then reconstructing $\dot{x}$ as $\dot{x} = \sigma\sqrt{p(x)}$ on the interval where $p(x) \geq 0$.

2.1 Integrating-factor representation

Equation (5) is linear with variable coefficients. Introducing the integrating factor

$$\mu_\sigma(x) = \exp\left(2\sigma \int_{x_*}^{x} \alpha(\xi)\,\mathrm{d}\xi\right), \tag{6}$$

one obtains

$$\frac{\mathrm{d}}{\mathrm{d}x}\big(p(x)\mu_\sigma(x)\big) = -2V'(x)\mu_\sigma(x), \tag{7}$$

and hence, for a reference point (x_0, v_0) with $v_0 \neq 0$ and $\sigma = \mathrm{sgn}(v_0)$,

$$p_\sigma(x) = \frac{1}{\mu_\sigma(x)}\left[v_0^2\mu_\sigma(x_0) - 2\int_{x_0}^{x} V'(s)\mu_\sigma(s)\,\mathrm{d}s\right]. \tag{8}$$

This representation is exact and requires only one quadrature once α is specified. Where the integral can be evaluated in closed form, Eq. (8) yields explicit analytic phase-plane curves.

Although Eq. (5) is smooth for fixed σ, the global motion cannot, in general, be represented by a single expression because the governing branch changes whenever the velocity changes sign.

Remark 1 (Admissible domain, turning points, and branch switching) On any trajectory segment with fixed velocity sign $\sigma = \mathrm{sgn}(\dot{x})$, the reconstruction $\dot{x} = \sigma\sqrt{p(x)}$ requires $p(x) \geq 0$. Accordingly, a branch solution $p_\sigma(x)$ obtained from Eq. (8) is physically admissible only on the interval (starting from the initial point) on which $p_\sigma(x) \geq 0$ holds.

A point x_T with $p(x_T) = 0$ corresponds to $\dot{x}(t_T) = 0$. In a purely sliding regime (no sticking), such a point is a *turning point* if $V'(x_T) \neq 0$: the motion reverses direction and the velocity sign flips. The matching between branches is then imposed by the natural continuity conditions

$$x(t_T^-) = x(t_T^+) = x_T, \qquad \dot{x}(t_T^-) = \dot{x}(t_T^+) = 0, \tag{9}$$

equivalently,

$$p_\sigma(x_T) = 0, \qquad p_{-\sigma}(x_T) = 0, \tag{10}$$

with σ replaced by $-\sigma$ after t_T. Practically, one matches monotone pieces by integrating Eq. (5) on a fixed-σ branch until the first zero x_T of p_σ is reached, then restarting Eq. (8) from $(x_0, v_0) = (x_T, 0)$ on the opposite branch. In this sense, the global solution should be considered as *piecewise* even when α and V are smooth, because the model is non-smooth through $|\dot{x}|$ and $\mathrm{sgn}(\dot{x})$.

Remark 2 (Piecewise time reconstruction) If the time history is required, it follows on each monotone segment from

$$\frac{\mathrm{d}x}{\mathrm{d}t} = \sigma\sqrt{p_\sigma(x)} \quad\Rightarrow\quad t - t_0 = \int_{x_0}^{x} \frac{\mathrm{d}\xi}{\sigma\sqrt{p_\sigma(\xi)}}. \tag{11}$$

This integral is evaluated separately on each segment and then matched across turning points, as described in Remark 1.

2.2 Common construction workflow

The three examples below follow the same construction (cf. Fig. 1). First, the saddle-type equilibria of the potential are identified. For each saddle, Eq. (8) is initialized with $p = 0$ and continued on a fixed velocity branch. The branch is followed until one of three cases occurs: a finite zero of p gives a turning point, another saddle-type equilibrium is reached, or no further finite zero exists, and the branch continues to infinity. At a turning point, the velocity sign is changed, and the next branch is initialized from the same position. The resulting branch matching gives the stable-manifold curve that forms the relevant basin boundary. Finally, the local integrity measure is obtained by minimizing the distance from the attractor to this boundary, including interior tangency points and finite endpoint candidates such as turning points or saddle connections.

3 Quadratic-cubic potential

We begin the examples with the confined asymmetric well

$$V(x) = \frac{1}{2}x^2 - \frac{1}{3}x^3, \qquad V'(x) = x - x^2, \tag{12}$$

which has a stable equilibrium at $x = 0$ and a barrier (saddle) at $x_s = 1$ (see Fig. 2).

This potential is not merely a convenient analytic test case: it represents the generic *lowest-order* approximation of a broad class of smooth *asymmetric* one-dimensional potentials near a stable equilibrium. Indeed, let $\widetilde{V}(x)$ be any C^3 potential with a stable equilibrium at $x = 0$, so that $\widetilde{V}'(0) = 0$ and $\widetilde{V}''(0) > 0$. A Taylor expansion about $x = 0$ gives

$$\widetilde{V}(x) = \widetilde{V}(0) + \frac{1}{2}\widetilde{V}''(0)\,x^2 + \frac{1}{6}\widetilde{V}^{(3)}(0)\,x^3 + \mathcal{O}(x^4), \tag{13}$$

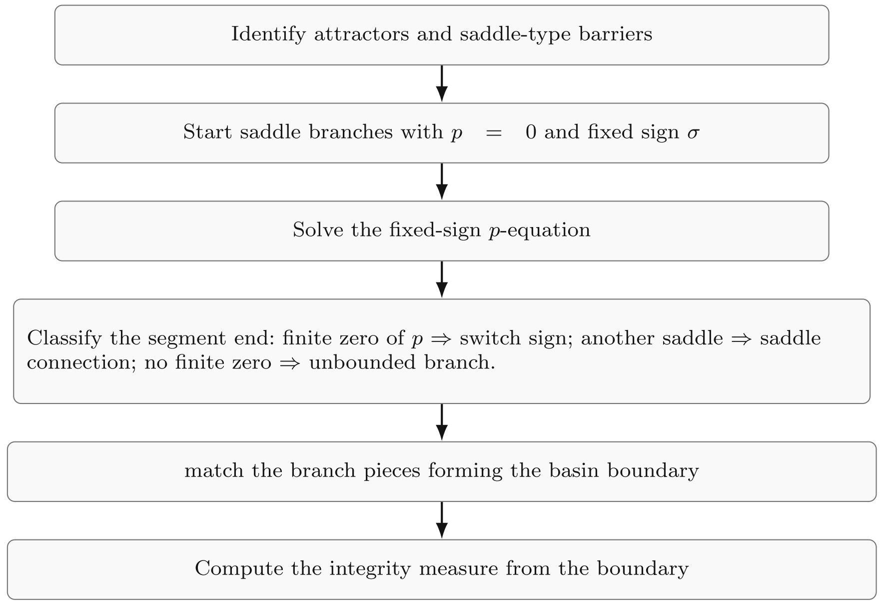

Fig. 1 Common workflow used in the examples. A fixed-sign segment either reaches a turning point, reaches another saddle, or continues without a further finite zero

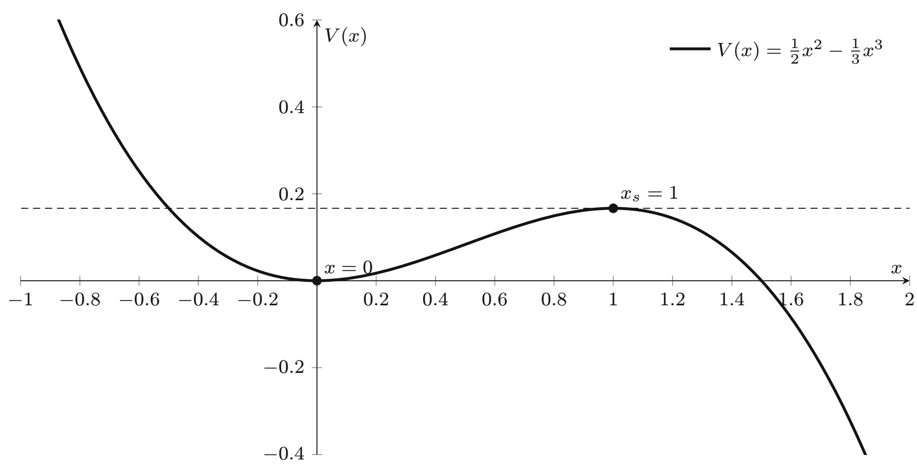

Fig. 2 Quadratic-cubic potential (12) with stable equilibrium at $x = 0$ and barrier at $x_s = 1$

where the constant $\widetilde{V}(0)$ is irrelevant for the dynamics. After scaling the displacement to normalize the quadratic stiffness, $x = \sqrt{\widetilde{V}''(0)}\,\xi$, and truncating beyond cubic order, one obtains the canonical form

$$V(\xi) = \frac{1}{2}\xi^2 + \frac{\kappa}{3}\xi^3, \qquad \kappa = \frac{\widetilde{V}^{(3)}(0)}{2\,\widetilde{V}''(0)^{3/2}}. \tag{14}$$

The sign of κ encodes the local asymmetry; choosing $\kappa = -1$ by the further rescaling $\xi = \eta/|\kappa|$ yields (12) (up to an inessential multiplicative factor in V). Thus, (12) is the normal-form potential capturing the leading-order deviation from symmetry: the harmonic term describes the linearized dynamics, while the cubic correction introduces the first non-linear asymmetry that generically generates a finite barrier and, hence, a well-defined escape (or capture) threshold. In this section, we consider the simplest case: *constant* quadratic drag,

$$\alpha(x) \equiv \alpha > 0, \tag{15}$$

so that Eq. (1) reduces to

$$\ddot{x} + \alpha|\dot{x}|\,\dot{x} + x - x^2 = 0. \tag{16}$$

3.1 Branchwise solutions

On each monotone branch with fixed velocity sign $\sigma \in \{+1, -1\}$, the reduction of Sect. 2 yields the linear equation

$$\begin{aligned} \frac{\mathrm{d}p}{\mathrm{d}x} + 2\alpha\sigma\, p &= -2V'(x) \\ &= 2(-x + x^2) \\ &= -2x + 2x^2, \quad p(x) := \dot{x}^2. \end{aligned} \tag{17}$$

Using the integrating factor $e^{2\alpha\sigma x}$, the solution starting at the turning point ($p(x_T) = 0$) can be written as

$$p_\sigma(x; x_T) = e^{-2\alpha\sigma x} \int_{x_T}^{x} (-2s + 2s^2)\, e^{2\alpha\sigma s}\, \mathrm{d}s. \tag{18}$$

A convenient, explicit antiderivative is obtained by defining

$$I_\sigma(x) := \int (-2x + 2x^2)\, e^{2\alpha\sigma x}\, \mathrm{d}x,$$
$$p_\sigma(x; x_T) = e^{-2\alpha\sigma x}\big[I_\sigma(x) - I_\sigma(x_T)\big]. \tag{19}$$

For a constant α, the primitives can be chosen as

$$I_+(x) = e^{2\alpha x}\, \frac{2\alpha^2 x^2 - 2\alpha^2 x - 2\alpha x + \alpha + 1}{2\alpha^3}, \tag{20}$$
$$I_-(x) = e^{-2\alpha x}\, \frac{-2\alpha^2 x^2 + 2\alpha^2 x - 2\alpha x + \alpha - 1}{2\alpha^3}. \tag{21}$$

Accordingly, the phase-plane curves are recovered as $v(x) = \dot{x} = \sigma\sqrt{p_\sigma(x)}$ on each branch.

3.2 Left turning point of the saddle separatrix and critical drag

We construct the separatrix branch that emanates from the saddle $x_s = 1$ in *backward* time towards the well, i.e., towards decreasing x. Along this branch the backward-time velocity is positive, hence $\sigma = +1$ and $p = p_+$ with $p(1) = 0$. From (19) we obtain

$$p_+(x; 1) = e^{-2\alpha x}\big[I_+(x) - I_+(1)\big], \tag{22}$$

so that possible turning points correspond to zeros of p_+, equivalently to solutions of

$$I_+(x) = I_+(1), \qquad x < 1. \tag{23}$$

To decide whether such a solution exists, we exploit monotonicity. By definition,

$$I_+'(x) = (-2x + 2x^2)\, e^{2\alpha x} = 2x(x-1)\, e^{2\alpha x}. \tag{24}$$

Since the exponential factor is strictly positive, the sign of I_+' is governed by $2x(x-1)$:

$$I_+'(x) > 0 \text{ for } x < 0, \qquad I_+'(x) < 0 \text{ for } 0 < x < 1,$$
$$I_+'(x) > 0 \text{ for } x > 1. \tag{25}$$

Consequently, I_+ is strictly increasing on $(-\infty, 0]$, strictly decreasing on $[0, 1]$, and therefore attains a *unique* local maximum at $x = 0$. Moreover, from Eq. (20) one has the limits

$$\lim_{x\to-\infty} I_+(x) = 0, \qquad I_+(0) = \frac{\alpha+1}{2\alpha^3} > 0. \tag{26}$$

Thus, for $x < 0$ the primitive approaches zero from above and increases strictly to $I_+(0)$. On $[0, 1]$, it decreases strictly from $I_+(0)$ to $I_+(1)$, so no value on this interval is taken twice.

Evaluating Eq. (20) at the saddle yields

$$I_+(1) = e^{2\alpha}\, \frac{1-\alpha}{2\alpha^3}. \tag{27}$$

The three alternatives are illustrated in Fig. 3. The plot shows the normalized primitive $I_+(x)/I_+(0)$ for representative values of α; the normalization is only for comparison between different drag coefficients and does not change the root condition (23). The markers at $x = 1$ indicate the saddle value $I_+(1)$ and show the sign change at $\alpha = 1$.

We now distinguish three cases:

Case 1: $0 < \alpha < 1$. Then $I_+(1) > 0$. Since $I_+(0) > I_+(1)$ (because I_+ strictly decreases on $[0, 1]$) and $\lim_{x\to-\infty} I_+(x) = 0 < I_+(1)$, continuity implies that the equation $I_+(x) = I_+(1)$ has *at least one* solution on $(-\infty, 0)$. By strict monotonicity of I_+ on $(-\infty, 0]$, this solution is in fact *unique*; denote it by $x_L < 0$. Therefore,

$$I_+(x) - I_+(1) \begin{cases} < 0, & x \to -\infty, \\ = 0, & x = x_L, \\ > 0, & x \in (x_L, 1), \end{cases} \tag{28}$$

and Eq. (22) shows that $p_+(x; 1)$ is positive on $(x_L, 1)$ and vanishes only at $x = x_L$ and $x = 1$. Thus, a left turning point exists and is uniquely defined by Eq. (23).

Case 2: $\alpha = 1$. Then $I_+(1) = 0$ while $I_+(x) > 0$ for all $x < 1$ (in particular $I_+(0) > 0$), and $I_+(x) \to 0$ only as $x \to -\infty$. Hence, Eq. (23) has no finite solution with $x < 1$: at $\alpha = 1$, the left branch has no finite turning point and therefore does not reverse inside the well.

Case 3: $\alpha > 1$. Then $I_+(1) < 0$. For $x < 0$, one has $I_+(x) > 0 > I_+(1)$, while for $0 \le x < 1$ the strict decrease of I_+ on $[0, 1]$ gives $I_+(x) > I_+(1)$. Therefore the equality $I_+(x) = I_+(1)$ cannot hold for any $x < 1$, and Eq. (22) implies $p_+(x; 1) > 0$ for all $x < 1$: no left turning point exists.

Combining the cases, a left turning point exists if and only if $I_+(1) > 0$, i.e.,

$$0 < \alpha < 1, \qquad \alpha_{\text{crit}} = 1. \tag{29}$$

For later use, it is convenient to record the turning-point equation explicitly by inserting Eq. (20) into Eq. (23), yielding the scalar transcendental condition

$$e^{2\alpha x_L}\Big(2\alpha^2 x_L^2 - 2\alpha^2 x_L - 2\alpha x_L + \alpha + 1\Big) = e^{2\alpha}(1-\alpha). \tag{30}$$

Fig. 3 Primitive I_+ used to determine the left turning point in the quadratic-cubic example. The vertical dotted lines mark the maximum at $x = 0$ and the saddle position $x_s = 1$. The saddle value is positive for $0 < \alpha < 1$, zero at $\alpha = 1$, and negative for $\alpha > 1$

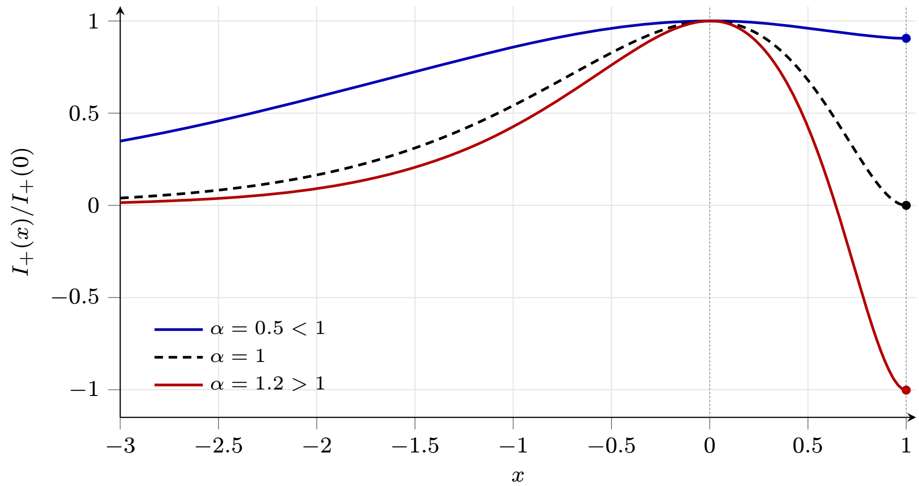

Following [55, 56], we denote by $W(\cdot; a_1, \ldots, a_n)$ any branch of the inverse of $u \mapsto e^u \prod_{j=1}^n (u - a_j)$, i.e., the generalized Lambert W function,

$$u = W(z; a_1, \ldots, a_n) \quad \Longleftrightarrow \quad e^u \prod_{j=1}^{n} (u - a_j) = z. \tag{31}$$

Thus, the turning-point condition (30) can be rewritten after one introduces the scaled variable

$$u := 2\alpha x, \qquad x = \frac{u}{2\alpha}. \tag{32}$$

Then, Eq. (30) becomes the quadratic-exponential equation

$$\Big(u^2 - 2(\alpha+1)u + 2(\alpha+1)\Big)e^u = 2(1-\alpha)e^{2\alpha}. \tag{33}$$

Factoring the quadratic,

$$\begin{aligned} &u^2 - 2(\alpha+1)u + 2(\alpha+1) = (u - a_1(\alpha))(u - a_2(\alpha)), \\ &a_{1,2}(\alpha) = (\alpha+1) \pm \sqrt{\alpha^2 - 1}, \end{aligned} \tag{34}$$

we obtain

$$(u - a_1(\alpha))(u - a_2(\alpha))\, e^u = 2(1-\alpha)e^{2\alpha}. \tag{35}$$

In terms of the generalized Lambert inverse $W(\cdot; a_1, a_2)$, defined implicitly by $e^u(u - a_1)(u - a_2) = z$, the turning point is therefore

$$\begin{aligned} u_L(\alpha) &= W_\kappa\Big(2(1-\alpha)e^{2\alpha};\ a_1(\alpha), a_2(\alpha)\Big), \\ x_L(\alpha) &= \frac{u_L(\alpha)}{2\alpha}. \end{aligned} \tag{36}$$

For $0 < \alpha < 1$, the parameters $a_{1,2}(\alpha)$ form a complex-conjugate pair, but the physically relevant *real* branch, denoted by W_κ, yields the real solution with $x_L(\alpha) < 0$ (equivalently $u_L(\alpha) < 0$), consistent with the uniqueness established above. Consequently, the endpoint candidate used later in the *LIM* construction, $r_{\text{end}}(\alpha) = |x_L(\alpha)| = -x_L(\alpha)$ for $0 < \alpha < 1$, can be written explicitly as

$$\begin{aligned} r_{\text{end}}(\alpha) = -\frac{1}{2\alpha}\, W_\kappa\Big(2(1-\alpha)e^{2\alpha};\ a_1(\alpha), a_2(\alpha)\Big), \\ 0 < \alpha < 1. \end{aligned} \tag{37}$$

The regular small-drag expansion of the left turning point is not needed for the basin construction itself. It is therefore given in Appendix A; the result is recorded in Eq. (131) and confirms that quadratic drag shifts the conservative turning point $x_L(0) = -1/2$ towards decreasing x.

3.3 Continuations to the right and phase-plane boundary

Once x_L is known (either from Eq. (30) or from Eq. (131)), the backward-time continuation from x_L to the right proceeds on the opposite velocity branch $\sigma = -1$, hence

$$\begin{aligned} p_-(x; x_L) &= e^{2\alpha x}\big[I_-(x) - I_-(x_L)\big], \\ v(x) &= -\sqrt{p_-(x; x_L)}. \end{aligned} \tag{38}$$

For completeness, the second branch of the saddle separatrix is obtained by continuing from $x_s = 1$ in backward time towards increasing x (thus $\sigma = -1$):

$$\begin{aligned} p_-(x; 1) &= e^{2\alpha x}\big[I_-(x) - I_-(1)\big], \\ v(x) &= -\sqrt{p_-(x; 1)}, \qquad x > 1. \end{aligned} \tag{39}$$

A finite right turning point $x_R > 1$ would satisfy $I_-(x_R) = I_-(1)$, after which the branch is continued with $\sigma = +1$ in the same way as in Eq. (38). For the potential (12),

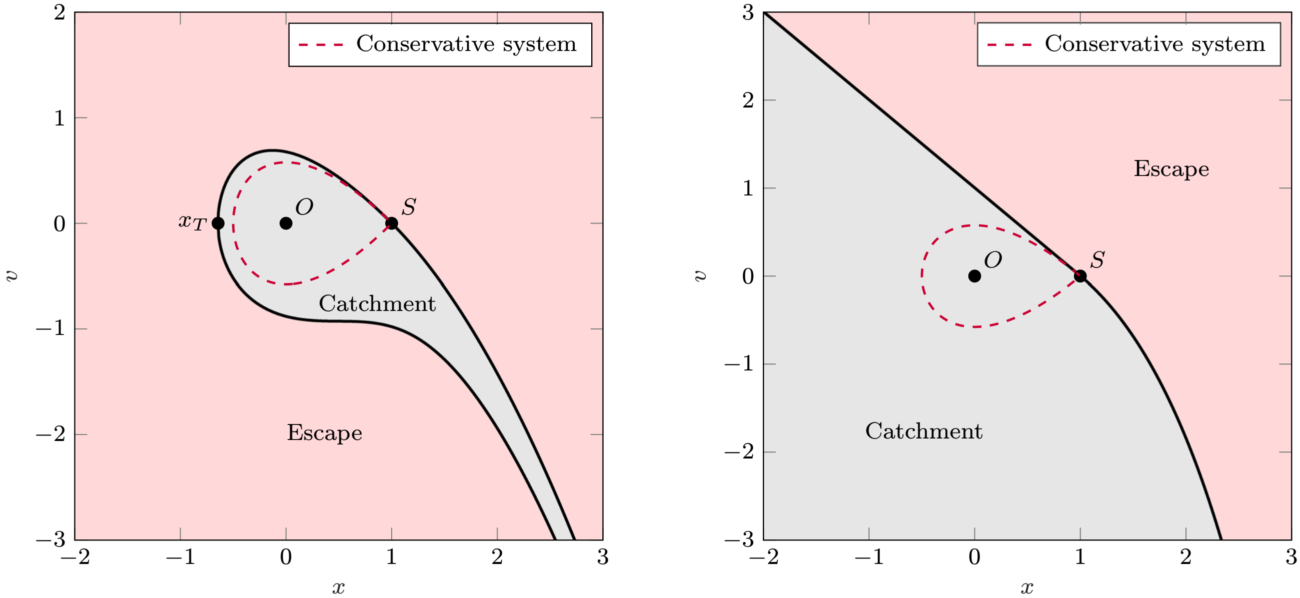

(a) $\alpha = 0.3$ (constant quadratic drag).

(b) $\alpha = 1 = \alpha_{\text{crit}}$: the finite left turning point vanishes.

Fig. 4 Asymmetric basin-of-attraction boundary verified by numerical time-domain simulations for two drag levels. The solid black curves are the analytically constructed separatrix branches. The shaded regions are obtained by numerically integrating Eq. (16) from a grid of initial conditions and classifying the long-time outcome. The stable attractor is located at the origin O, while the saddle point S is located at $(1, 0)$

$I'_{-}(x) = 2x(x-1)e^{-2\alpha x} > 0$ for $x > 1$, hence no finite x_R occurs and the saddle branch remains monotone, providing the remaining part of the basin of attraction's boundary on the escape side.

Together, Eq. (22) and Eq. (38) provide an explicit parametrization of the (asymmetric) basin-of-attraction boundary in the (x, v) plane for Eq. (16), assembled branch-wise as described in Sect. 2. Figure 4 compares this analytical boundary with direct numerical integration of the original second-order equation. In this notation, x_T denotes a turning point, i.e., a point where $p(x_T) = 0$. For the left branch in Fig. 4a, this finite turning point is $x_T = x_L(\alpha)$; for $\alpha = 1$ in Fig. 4b, no finite left turning point exists.

3.4 Polar form of the $\sigma = +1$ saddle branch and local integrity measure

We measure the *local integrity measure* as the minimal Euclidean distance from the stable attractor $(x, \dot{x}) = (0, 0)$ to the basin boundary in the phase plane (cf. [47–50]). On the quadratic-cubic potential with constant quadratic drag, the relevant boundary curve is generated by the separatrix branch emerging from the saddle $(x_s, \dot{x}) = (1, 0)$, with $\sigma = +1$ on its first monotone segment.

Introduce polar coordinates centered at the equilibrium,

$$x = r\cos\theta, \qquad \dot{x} = r\sin\theta, \qquad r \geq 0, \tag{40}$$

and consider the $\sigma = +1$ segment for which $\dot{x} \geq 0$ and thus $\theta \in [0, \pi]$. Along this segment the curve is given by $\dot{x} = +\sqrt{p_+(x; 1)}$, hence

$$r(x) = \sqrt{x^2 + p_+(x; 1)}, \qquad \theta(x) = \operatorname{atan2}\left(\sqrt{p_+(x; 1)},\ x\right), \tag{41}$$

or, equivalently, by the implicit polar relation

$$r(\theta)^2 \sin^2\theta = p_+\big(r(\theta)\cos\theta;\ 1\big), \qquad \theta \in [0, \pi]. \tag{42}$$

For later use, we recall the explicit saddle-started expression (obtained from $p(1) = 0$):

$$p_+(x; 1) = \frac{1}{2\alpha^3}\Big(2\alpha^2 x^2 - 2\alpha^2 x - 2\alpha x + \alpha + 1 - (1-\alpha)e^{2\alpha(1-x)}\Big), \qquad p_+(1; 1) = 0. \tag{43}$$

3.5 Two competing minimizers: interior tangency vs. boundary at $\theta = \pi$

The minimum of r along the $\sigma = +1$ curve must be sought on the *finite* parameter interval where that segment exists. For $0 < \alpha < 1$, the $\sigma = +1$ segment runs from the left turning point $x_L(\alpha) < 0$ (where $\dot{x} = 0$ and thus $\theta = \pi$) to the saddle at $x = 1$ (where $\theta = 0$). Consequently, the minimizer of r can occur either at an interior stationary point of $r(x)$ (equivalently, tangency of the curve to a circle centered at the origin), or at the boundary point $x = x_L$ (i.e., at $\theta = \pi$).

3.5.1 Interior stationary point and tangency

Minimizing $r^2(x) = x^2 + p_+(x;1)$, and using the branch equation $p' + 2\alpha p = -2V'(x)$ with $V'(x) = x - x^2$, yields

$$\frac{\mathrm{d}}{\mathrm{d}x}\big(r^2(x)\big) = 2x + p'_+(x;1) = 2\big(x^2 - \alpha\, p_+(x;1)\big). \tag{44}$$

Hence, an interior extremum satisfies

$$\alpha\, p_+(x_*;1) = x_*^2, \quad \Longleftrightarrow \quad \dot{x}_* = \sqrt{p_+(x_*;1)} = \frac{|x_*|}{\sqrt{\alpha}}, \tag{45}$$

which in polar form fixes the ray of extremality by $\tan\theta_* = \alpha^{-1/2}$ (for $x_* > 0$). Substituting Eq. (43) into Eq. (45) gives

$$(1-\alpha)e^{2\alpha(1-x_*)} = (1+\alpha)\big(1 - 2\alpha x_*\big), \tag{46}$$

which can be solved explicitly using the Lambert W function. Define

$$D(\alpha) := \frac{\alpha - 1}{\alpha + 1}\, e^{2\alpha - 1}. \tag{47}$$

Then

$$x_*(\alpha) = \frac{1 + W_k\big(D(\alpha)\big)}{2\alpha}. \tag{48}$$

For $0 < \alpha < 1$, one has $D(\alpha) \in (-1/e, 0)$, so there are two real branches ($k \in \{0, 1\}$). The *relevant* interior minimum corresponds to the principal branch W_0 and satisfies $x_{\min} \in (0, 1)$:

$$\begin{aligned} x_{\min}(\alpha) &= \frac{1 + W_0\big(D(\alpha)\big)}{2\alpha}, \\ \theta_{\min}(\alpha) &= \arctan\big(\alpha^{-1/2}\big) \in \big(0, \tfrac{\pi}{2}\big). \end{aligned} \tag{49}$$

At this point Eq. (45) implies $p_+(x_{\min};1) = x_{\min}^2/\alpha$, hence the associated radius is

$$\begin{aligned} r_{\text{int}}(\alpha) &= \sqrt{x_{\min}(\alpha)^2 + p_+(x_{\min}(\alpha);1)} = x_{\min}(\alpha)\sqrt{1 + \frac{1}{\alpha}} \\ &= \frac{1 + W_0\big(D(\alpha)\big)}{2\alpha}\sqrt{1 + \frac{1}{\alpha}}. \end{aligned} \tag{50}$$

Geometrically, the circle $r = r_{\text{int}}(\alpha)$ is tangent to the $\sigma = +1$ branch at $(x, \dot{x}) = (x_{\min}, x_{\min}/\sqrt{\alpha})$.

3.5.2 Boundary point at $\theta = \pi$ (turning point)

When $0 < \alpha < 1$ the $\sigma = +1$ segment begins at the left turning point $x_L(\alpha) < 0$ where $p_+(x_L;1) = 0$ and thus $\dot{x} = 0$ and $\theta = \pi$. The radius there is

$$r_{\text{end}}(\alpha) = \sqrt{x_L(\alpha)^2 + 0} = |x_L(\alpha)| = -x_L(\alpha), \tag{51}$$

where x_L is the unique solution $x_L < 1$ of $p_+(x_L;1) = 0$. Equivalently, $x_L(\alpha)$ admits the explicit generalized Lambert W representation (36), and thus $r_{\text{end}}(\alpha)$ is given in closed form by Eq. (37).

This candidate is missed if one only enforces the stationary condition (45), and it becomes decisive for sufficiently small α. The local integrity measure is therefore

$$r_{\text{loc}}(\alpha) = \begin{cases} \min\{\, r_{\text{end}}(\alpha),\ r_{\text{int}}(\alpha)\,\}, & 0 < \alpha < 1, \\ r_{\text{int}}(\alpha), & \alpha \geq 1, \end{cases} \tag{52}$$

where r_{int} is given explicitly by Eq. (50), while r_{end} is determined implicitly via x_L. Moreover, there is a unique transition value $\alpha = \alpha^\dagger \in (0, 1)$ at which the two candidates coincide,

$$r_{\text{end}}(\alpha^\dagger) = r_{\text{int}}(\alpha^\dagger), \tag{53}$$

so that the minimizer shifts from the turning-point boundary ($\theta = \pi$) to the interior tangency point. Numerically, one finds

$$\alpha^\dagger \approx 0.27944, \tag{54}$$

with $r_{\text{loc}}(\alpha) = r_{\text{end}}(\alpha)$ for $0 < \alpha < \alpha^\dagger$ and $r_{\text{loc}}(\alpha) = r_{\text{int}}(\alpha)$ for $\alpha^\dagger < \alpha < 1$. For a graphical representation of $r_{\text{loc}}(\alpha)$, see Fig. 5. In Fig. 6, the phase space trajectory and the *LIM* are depicted for $\alpha^\dagger$.

4 Bistable Duffing potential

We next consider the symmetric bistable Duffing potential

$$V(x) = -\frac{x^2}{2} + \frac{x^4}{4}, \qquad V'(x) = -x + x^3, \tag{55}$$

which has two stable equilibria at $x = \pm 1$ and a barrier (saddle) at $x_s = 0$ (see Fig. 7). In the present setting, we take

$$\alpha(x) \equiv \alpha > 0, \tag{56}$$

so that Eq. (1) reduces to

$$\begin{aligned} &\ddot{x} + \alpha|\dot{x}|\,\dot{x} + V'(x) = 0 \quad \Longleftrightarrow \quad \ddot{x} + \alpha|\dot{x}|\,\dot{x} - x + x^3 \\ &= 0. \end{aligned} \tag{57}$$

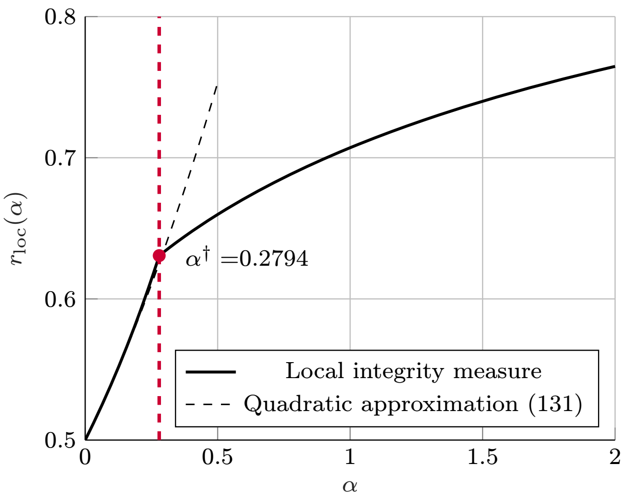

Fig. 5 Local integrity measure $r_{\mathrm{loc}}(\alpha)$ in the quadratic-cubic potential, computed as the minimum of the interior tangency radius and the endpoint radius

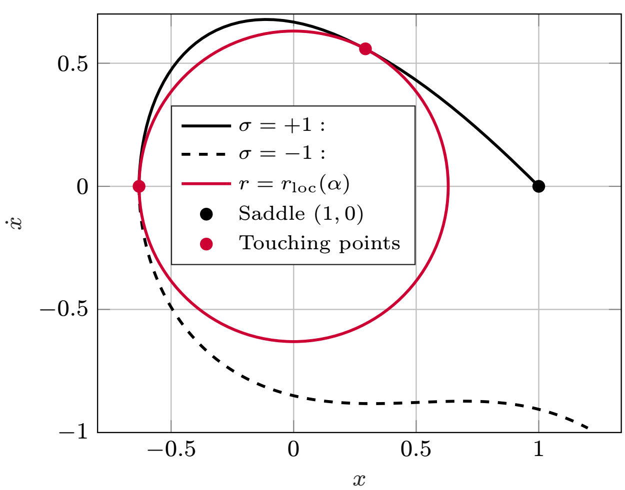

Fig. 6 Local integrity measure $r_{\mathrm{loc}}(\alpha)$ at the switching point $\alpha^\dagger \approx 0.27944$.

The basin boundary between capture in the left versus the right well is given by the stable manifold of the saddle $x_s = 0$, which is obtained explicitly in the phase plane by evaluating the branchwise solution $p_\sigma(x) = \dot{x}^2$.

4.1 Branchwise closed form for $p_\sigma(x)$

On a branch of fixed velocity sign $\sigma = \operatorname{sgn}(\dot{x}) \in \{+1, -1\}$, the reduced equation for $p_\sigma(x) = \dot{x}^2$ reads

$$\frac{\mathrm{d}p}{\mathrm{d}x} + 2\alpha\sigma\, p = 2x - 2x^3, \tag{58}$$

and a turning point x_T is characterized by $p(x_T) = 0$. Using the integrating factor $e^{2\alpha\sigma x}$ and the condition $p(x_T) = 0$ gives the integral representation

$$p_\sigma(x; x_T) = e^{-2\alpha\sigma x} \int_{x_T}^{x} \left(2s - 2s^3\right) e^{2\alpha\sigma s}\, \mathrm{d}s. \tag{59}$$

Define the primitive

$$\begin{aligned} I_\sigma(x) &:= \int \left(2x - 2x^3\right) e^{2\alpha\sigma x}\, \mathrm{d}x, \\ F_\sigma(x; x_T) &:= I_\sigma(x) - I_\sigma(x_T), \end{aligned} \tag{60}$$

so that

$$p_\sigma(x; x_T) = e^{-2\alpha\sigma x} F_\sigma(x; x_T). \tag{61}$$

Since the exponential factor never vanishes, zeros of p_σ coincide with zeros of F_σ. A direct evaluation yields

$$I_+(x) = e^{2\alpha x} \frac{-4\alpha^3 x^3 + 4\alpha^3 x + 6\alpha^2 x^2 - 2\alpha^2 - 6\alpha x + 3}{4\alpha^4}, \tag{62}$$

$$I_-(x) = e^{-2\alpha x} \frac{4\alpha^3 x^3 - 4\alpha^3 x + 6\alpha^2 x^2 - 2\alpha^2 + 6\alpha x + 3}{4\alpha^4}. \tag{63}$$

It is convenient to denote the upper- and lower-half-plane branches by

$$p_L(x; x_T) := p_+(x; x_T) = e^{-2\alpha x}\left(I_+(x) - I_+(x_T)\right), \tag{64}$$

$$p_R(x; x_T) := p_-(x; x_T) = e^{+2\alpha x}\left(I_-(x) - I_-(x_T)\right), \tag{65}$$

with the associated velocity graphs

$$\begin{aligned} \dot{x} &= +\sqrt{p_L(x; x_T)} \quad (\dot{x} > 0), \\ \dot{x} &= -\sqrt{p_R(x; x_T)} \quad (\dot{x} < 0), \end{aligned} \tag{66}$$

restricted to the admissible domain where $p \geq 0$.

4.2 Separatrix construction by turning-point matching

The saddle separatrix is generated by the stable manifold of $(x, \dot{x}) = (0, 0)$. Starting from the saddle as an initial turning point

$$x_T^{(0)} = 0, \qquad p(x_T^{(0)}) = 0, \tag{67}$$

one follows the trajectory in backward time. On each monotone segment, the phase-plane curve is given by Eq. (61) with a fixed sign σ. The next turning point x_{k+1} is obtained as a root of

$$F_\sigma(x_{k+1}; x_k) = I_\sigma(x_{k+1}) - I_\sigma(x_k) = 0, \tag{68}$$

Fig. 7 Symmetric bistable Duffing potential $V(x) = -\frac{x^2}{2} + \frac{x^4}{4}$ with stable equilibria at $x = \pm 1$ and barrier at $x_s = 0$

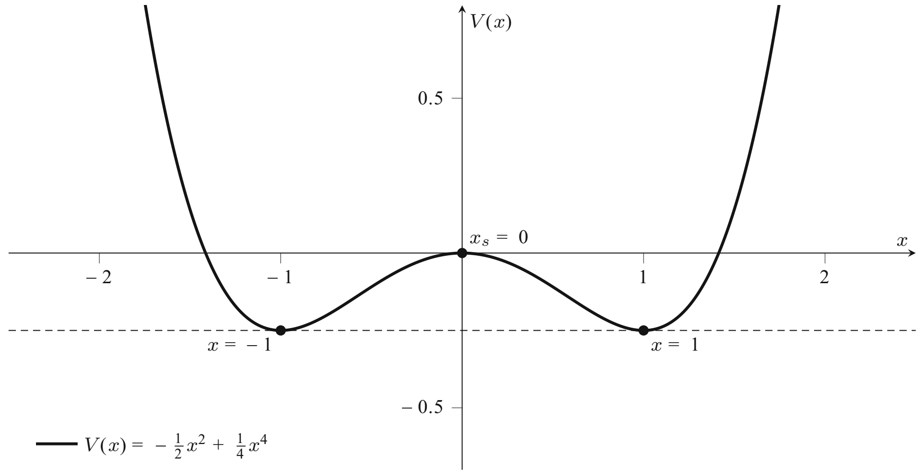

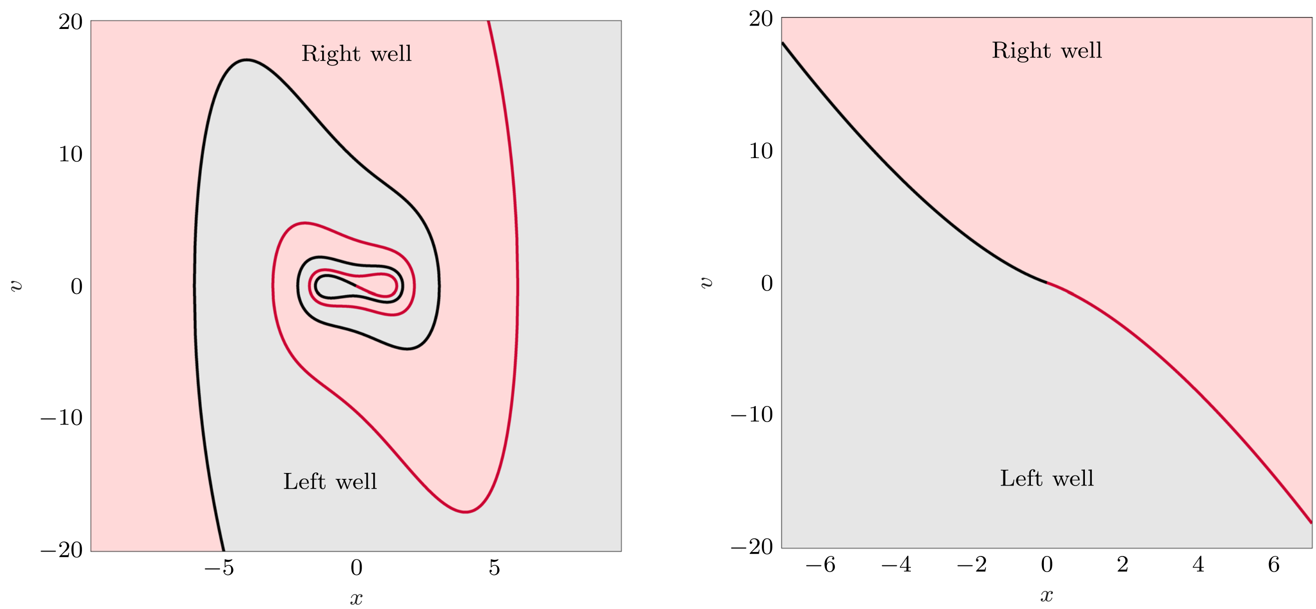

(a) $\alpha = 0.2$

(b) $\alpha = \sqrt{3/2}$

Fig. 8 Analytically calculated basin-of-attraction boundaries validated against numerical data (filled area)

lying on the opposite side of the origin. At each turning point one updates $x_T \leftarrow x_{k+1}$ and switches branch $\sigma \mapsto -\sigma$. Iterating this produces a sequence of alternating turning points and a matched separatrix curve in the $(x, \dot{x})$ plane. Carrying out the procedure once with $\sigma = +1$ on the first segment and once with $\sigma = -1$ yields the two symmetric saddle trajectories separating the two distinct basins of attraction (see Fig. 8).

4.3 Last turning points and the critical condition

For a given turning point x_T on a branch, a further turning point in backward time exists on the opposite side if and only if $F_\sigma(\cdot; x_T)$ changes sign there. This is encoded by the sign of $I_\sigma(x_T)$ together with the fact that $I_+(x) \to 0$ as $x \to -\infty$ and $I_-(x) \to 0$ as $x \to +\infty$ (the exponential factors dominate polynomial growth). Consequently, the *limiting* (outermost) turning points satisfy

$$I_+(x_T) = 0 \quad \text{(left branch)}, \qquad I_-(x_T) = 0 \quad \text{(right branch)}. \tag{69}$$

Using Eqs. (62)–(63), these conditions reduce to cubic equations

$$P_+(x_T, \alpha) = 0, \qquad P_-(x_T, \alpha) = 0, \tag{70}$$

where

$$P_+(x,\alpha) := -4\alpha^3x^3 + 4\alpha^3x + 6\alpha^2x^2 - 2\alpha^2 - 6\alpha x + 3, \tag{71}$$

$$P_-(x,\alpha) := 4\alpha^3x^3 - 4\alpha^3x + 6\alpha^2x^2 - 2\alpha^2 + 6\alpha x + 3. \tag{72}$$

The relevant real roots define the terminal turning points reached in backward time before the separatrix continues monotonically to large $|x|$ on that last branch.

4.4 Closed form for the critical turning point

Solving $P_+(x_T,\alpha) = 0$ yields an explicit expression for the outermost turning point $x_T^{\mathrm{crit}}(\alpha) > 0$. Dividing $P_+ = 0$ by $-4\alpha^3$ and shifting

$$x_T = y + \frac{1}{2\alpha}, \tag{73}$$

one obtains the depressed cubic

$$y^3 + p(\alpha)y + q(\alpha) = 0, \qquad p(\alpha) = \frac{3-4\alpha^2}{4\alpha^2},$$
$$q(\alpha) = -\frac{1}{4\alpha^3}, \tag{74}$$

with discriminant

$$\Delta(\alpha) = \left(\frac{q}{2}\right)^2 + \left(\frac{p}{3}\right)^3 = \frac{27-\left(4\alpha^2-3\right)^3}{1728\,\alpha^6}. \tag{75}$$

Accordingly, $\Delta(\alpha) \geq 0$ for $0 < \alpha \leq \sqrt{3/2}$ and $\Delta(\alpha) < 0$ for $\alpha > \sqrt{3/2}$.

4.4.1 Case $\Delta(\alpha) \geq 0$ ($0 < \alpha \leq \sqrt{3/2}$): Cardano form

Define

$$A(\alpha) := -\frac{q}{2} = \frac{1}{8\alpha^3}, \qquad B(\alpha) := \sqrt{\Delta(\alpha)}$$
$$= \frac{\sqrt{27-\left(4\alpha^2-3\right)^3}}{24\sqrt{3}\,\alpha^3}. \tag{76}$$

Then the unique real root of Eq. (74) is

$$y(\alpha) = \sqrt[3]{A(\alpha)+B(\alpha)} + \sqrt[3]{A(\alpha)-B(\alpha)}, \tag{77}$$

and therefore

$$x_T^{\mathrm{crit}}(\alpha) = \frac{1}{2\alpha} + \sqrt[3]{\frac{1}{8\alpha^3} + \frac{\sqrt{27-(4\alpha^2-3)^3}}{24\sqrt{3}\,\alpha^3}}$$
$$+\sqrt[3]{\frac{1}{8\alpha^3} - \frac{\sqrt{27-(4\alpha^2-3)^3}}{24\sqrt{3}\,\alpha^3}}. \tag{78}$$

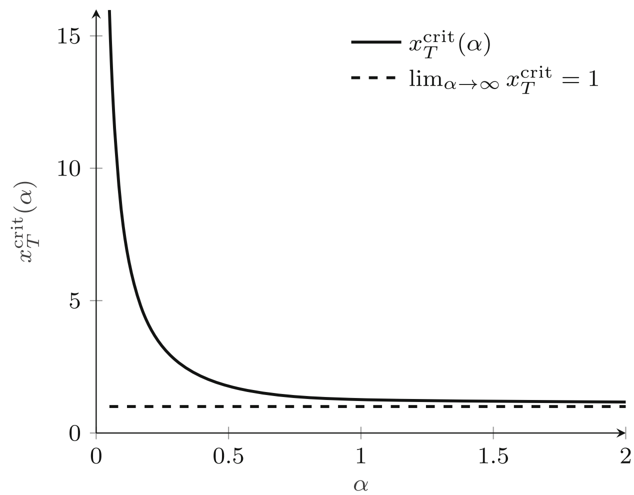

Fig. 9 The location of the last turning point x_T as a function of α

4.4.2 Case $\Delta(\alpha) < 0$ ($\alpha > \sqrt{3/2}$): trigonometric form (largest positive root)

In this regime, $p(\alpha) < 0$ and Eq. (74) has three real roots. Writing

$$\rho(\alpha) = 2\sqrt{-\frac{p(\alpha)}{3}} = \frac{\sqrt{4\alpha^2-3}}{\sqrt{3}\,\alpha},$$
$$\varphi(\alpha) = \arccos\left(\frac{3\sqrt{3}}{(4\alpha^2-3)^{3/2}}\right), \tag{79}$$

the largest real root is

$$y(\alpha) = \rho(\alpha)\cos\left(\frac{\varphi(\alpha)}{3}\right), \tag{80}$$

hence

$$x_T^{\mathrm{crit}}(\alpha) = \frac{1}{2\alpha} + \frac{\sqrt{4\alpha^2-3}}{\sqrt{3}\,\alpha}$$
$$\cos\left(\frac{1}{3}\arccos\left(\frac{3\sqrt{3}}{(4\alpha^2-3)^{3/2}}\right)\right), \quad \alpha > \sqrt{\frac{3}{2}}. \tag{81}$$

The location of the last turning point is shown as a function of α in Fig. 9. By symmetry of (57) under $(x,\dot{x}) \mapsto (-x,-\dot{x})$, the corresponding critical turning point on the negative side satisfies

$$x_{T,\mathrm{left}}^{\mathrm{crit}}(\alpha) = -x_T^{\mathrm{crit}}(\alpha). \tag{82}$$

This result means that the number of turning points of the saddle separatrix is finite for any $\alpha > 0$. It is possible to

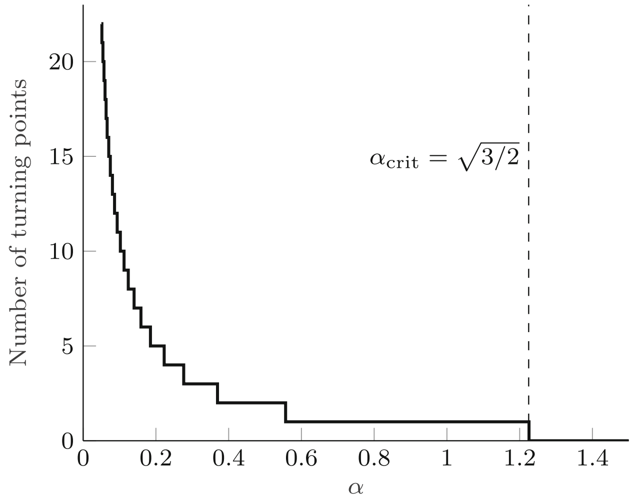

Fig. 10 Numerically determined number of turning points of the saddle separatrix as a function of α

determine their number for any values of α numerically (see Fig. 10). Specifically, for $\alpha > \sqrt{3/2}$, there are no over-the-well oscillations: any trajectory falls directly into one or the other well. Within a well, of course, oscillations are possible, but the motion is contained in the corresponding well for all times.

4.5 Local integrity measure about the left attractor via generalized Lambert *W* functions

We consider the left attractor $E_- := (-1, 0)$ of the bistable Duffing system with quadratic drag $\alpha(x) \equiv \alpha > 0$. The *local integrity measure* (*LIM*) about E_- is defined as the minimal Euclidean distance from E_- to the saddle separatrix $\mathcal{S}$ (the basin boundary),

$$r_{\mathrm{loc},-}(\alpha) := \min_{(x,\dot{x})\in\mathcal{S}} \sqrt{(x+1)^2 + \dot{x}^{\,2}}. \tag{83}$$

As in the quadratic-cubic case, the minimizer is either an interior tangency point of the distance circle to the separatrix graph, or a finite endpoint of the saddle branch (a turning point), hence the resulting $r_{\mathrm{loc},-}(\alpha)$ is generically *piecewise*.

4.5.1 Saddle branch towards the left well

The upper separatrix segment leaving the saddle $(0, 0)$ in backward time towards the left well satisfies $\sigma = +1$ and $p(0) = 0$. Using the explicit primitive $I_+(x)$ from Eq. (62) gives

$$\begin{aligned} p_+(x;0) &= e^{-2\alpha x}\big(I_+(x) - I_+(0)\big), \\ I_+(0) &= \frac{3-2\alpha^2}{4\alpha^4}, \end{aligned} \tag{84}$$

or, equivalently, the explicit closed form

$$\begin{aligned} p_+(x;0) = \frac{1}{4\alpha^4}\Big(&-4\alpha^3x^3 + 6\alpha^2x^2 + (4\alpha^3 - 6\alpha)x \\ &+(3-2\alpha^2) - (3-2\alpha^2)e^{-2\alpha x}\Big). \end{aligned} \tag{85}$$

Along this branch, the squared distance to E_- reads

$$r^2(x;\alpha) = (x+1)^2 + p_+(x;0). \tag{86}$$

4.5.2 Interior minimizer (tangency) and generalized W_2

Any interior minimizer x_* satisfies $\frac{\mathrm{d}}{\mathrm{d}x} r^2(x;\alpha) = 0$, i.e., $2(x_* + 1) + p_+'(x_*;0) = 0$. Using the branch equation $p_+' + 2\alpha p_+ = 2x - 2x^3$ (for $\sigma = +1$) yields the tangency relation

$$\alpha\, p_+(x_*;0) = 2x_* + 1 - x_*^3. \tag{87}$$

Substituting Eq. (85) into Eq. (87) gives

$$\begin{aligned} Q(x_*;\alpha)\, e^{2\alpha x_*} = 3 - 2\alpha^2, \qquad Q(x;\alpha) := 6\alpha^2x^2 \\ -(4\alpha^3 + 6\alpha)x + (3 - 2\alpha^2 - 4\alpha^3), \end{aligned} \tag{88}$$

i.e., a quadratic polynomial times an exponential. Introducing $u := 2\alpha x$ transforms (88) into

$$\big(u^2 - A(\alpha)u + B(\alpha)\big)\, e^u = K(\alpha), \tag{89}$$

with

$$\begin{aligned} A(\alpha) &= 2 + \frac{4}{3}\alpha^2, \\ B(\alpha) &= 2 - \frac{4}{3}\alpha^2 - \frac{8}{3}\alpha^3, \\ K(\alpha) &= 2 - \frac{4}{3}\alpha^2. \end{aligned} \tag{90}$$

Factoring $u^2 - Au + B = (u - u_1)(u - u_2)$ with

$$u_{1,2}(\alpha) = \frac{A(\alpha) \pm \sqrt{A(\alpha)^2 - 4B(\alpha)}}{2}, \tag{91}$$

Eq. (89) becomes

$$(u - u_1(\alpha))(u - u_2(\alpha))\, e^u = K(\alpha). \tag{92}$$

With the previously introduced notation in (31), the tangency location admits the generalized-W representation

$$u_*(\alpha) = W\big(K(\alpha);\ u_1(\alpha), u_2(\alpha)\big), \qquad x_*(\alpha) = \frac{u_*(\alpha)}{2\alpha}, \tag{93}$$

where the physically relevant branch is selected by the constraint $x_*(\alpha) \in \mathcal{I}(\alpha)$, the admissible interval of the saddle branch (i.e., where $p_+(x;0) \geq 0$ and $x < 0$ for the left-well *LIM*). At $x = x_*$, Eq. (87) gives $p_+(x_*;0) = (2x_* + 1 - x_*^3)/\alpha$, hence the tangency radius is

$$r_{\text{int}}^2(\alpha) = (x_*(\alpha) + 1)^2 + \frac{2x_*(\alpha) + 1 - x_*(\alpha)^3}{\alpha}. \tag{94}$$

4.5.3 Endpoint candidate (turning point) and generalized W_3

If the saddle branch has a finite left turning point $x_L(\alpha) < 0$ (i.e., $p_+(x_L;0) = 0$), then the endpoint distance is

$$r_{\text{end}}(\alpha) = |x_L(\alpha) + 1|. \tag{95}$$

The turning point condition $p_+(x_L;0) = 0$ is equivalent to Eq. (85) with $p_+ = 0$, i.e.,

$$\Big(-4\alpha^3 x_L^3 + 6\alpha^2 x_L^2 + (4\alpha^3 - 6\alpha)x_L + (3 - 2\alpha^2)\Big)e^{2\alpha x_L} = 3 - 2\alpha^2. \tag{96}$$

Introducing $u_L := 2\alpha x_L$, we can rewrite Eq. (96) as a cubic polynomial in u_L times e^{u_L}:

$$P(u_L;\alpha)\, e^{u_L} = K_3(\alpha), \tag{97}$$

where

$$P(u;\alpha) = u^3 - 3u^2 + (6 - 4\alpha^2)u + (4\alpha^2 - 6), \quad K_3(\alpha) = 4\alpha^2 - 6. \tag{98}$$

Note that $u = 0$ always solves Eq. (97) (since $P(0;\alpha) = K_3(\alpha)$), corresponding to the saddle point $x = 0$; the relevant endpoint for the left-well branch is a *nontrivial* solution $u_L < 0$, when it exists. In particular, additional real branches of Eq. (97) (beyond $u = 0$) occur only for

$$K_3(\alpha) < 0 \iff 0 < \alpha < \sqrt{\tfrac{3}{2}}, \tag{99}$$

while for $\alpha \geq \sqrt{3/2}$ the saddle branch extends leftwards without a finite turning point, and the endpoint candidate given by Eq. (95) is absent. Factoring $P(u;\alpha) = (u - a_1(\alpha))(u - a_2(\alpha))(u - a_3(\alpha))$, Eq. (97) is of generalized Lambert type, and the turning-point location can be represented as

$$u_L(\alpha) = W\big(K_3(\alpha);\, a_1(\alpha), a_2(\alpha), a_3(\alpha)\big), \quad x_L(\alpha) = \frac{u_L(\alpha)}{2\alpha}, \tag{100}$$

where the physically relevant branch is selected by $u_L(\alpha) < 0$ (hence $x_L < 0$) and by admissibility of the saddle branch.

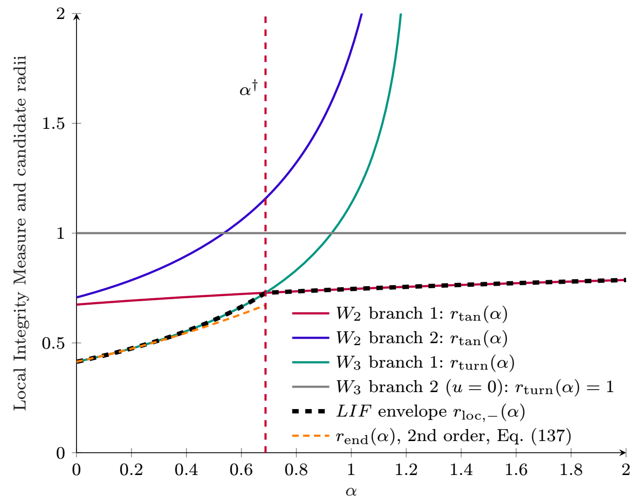

Fig. 11 Local integrity measure as a function of α for the symmetric double-well Duffing potential

4.5.4 Intersection of the active W_2 and W_3 radii and kink location

The *LIM* is the lower envelope of admissible candidates, so the "kink" occurs when the active minimizer switches from the endpoint to the interior tangency. This transition $\alpha^\dagger \in (0, \sqrt{3/2})$ is therefore characterized by

$$r_{\text{int}}(\alpha^\dagger) = r_{\text{end}}(\alpha^\dagger). \tag{101}$$

Writing $x = u/(2\alpha)$ in Eq. (94) and using Eq. (95) yields the explicit scalar equation

$$\Phi(\alpha) := \left(1 + \frac{u_*(\alpha)}{2\alpha}\right)^2 + \frac{u_*(\alpha)}{\alpha^2} + \frac{1}{\alpha} - \frac{u_*(\alpha)^3}{8\alpha^4} - \left(1 + \frac{u_L(\alpha)}{2\alpha}\right)^2 = 0, \qquad \alpha \in \left(0, \sqrt{\tfrac{3}{2}}\right), \tag{102}$$

where $u_*(\alpha)$ is the admissible real generalized-W_2 branch solving Eq. (92) (so $u_*(\alpha) = 2\alpha x_*(\alpha)$), and $u_L(\alpha)$ is the admissible real nontrivial generalized-W_3 branch solving Eq. (97) (so $u_L(\alpha) = 2\alpha x_L(\alpha) < 0$). Solving Eq. (102) gives the crossover value

$$\alpha^\dagger \approx 0.6878800931, \quad r_{\text{int}}(\alpha^\dagger) = r_{\text{end}}(\alpha^\dagger) \approx 0.7281930999, \tag{103}$$

and hence $r_{\text{loc},-}(\alpha)$ is endpoint-controlled for $0 < \alpha < \alpha^\dagger$ and tangency-controlled for $\alpha^\dagger < \alpha < \sqrt{3/2}$. For a graphical representation of $r_{\text{loc},-}(\alpha)$, see Fig. 11. For the limiting case $\alpha^\dagger$, the *LIM*-circle is tangential at two points to the separatrix (see Fig. 12).

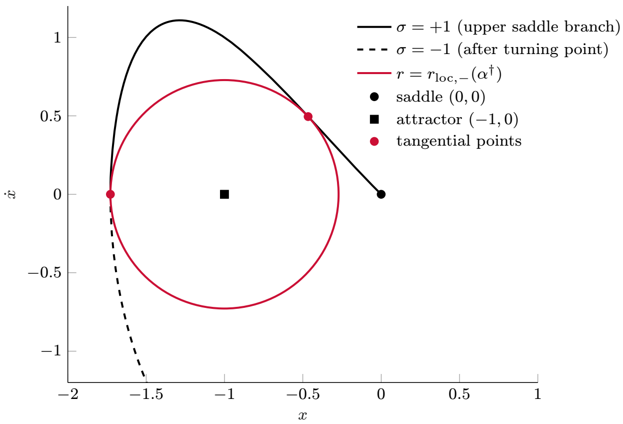

Fig. 12 Borderline double-contact case at $\alpha = \alpha^\dagger \approx 0.6878800931$: the minimal-distance circle centered at $E_- = (-1, 0)$ touches the saddle separatrix $\mathcal{S}$ at two points simultaneously (the left turning-point endpoint and an interior tangency point). This marks the switch from endpoint-controlled to tangency-controlled $r_{\mathrm{loc},-}(\alpha)$. At $\alpha^\dagger$ the common radius is $r_{\mathrm{int}}(\alpha^\dagger) = r_{\mathrm{end}}(\alpha^\dagger) \approx 0.7281930999$

The corresponding small-drag expansion of the endpoint candidate is used only as an asymptotic check. To keep the main text focused on the exact basin construction, the coefficient matching is moved to Appendix A; the endpoint approximation is given in Eq. (137).

5 Quadratic-quartic potential

We finally consider the confined symmetric well with two barriers

$$V(x) = \frac{1}{2}x^2 - \frac{1}{4}x^4, \qquad V'(x) = x - x^3, \tag{104}$$

which has a stable equilibrium at $x = 0$ and two saddles at $x = \pm 1$ (with barrier height $V(\pm 1) = 1/4$, see Fig. 13). With constant quadratic drag

$$\alpha(x) \equiv \alpha > 0, \tag{105}$$

the equation of motion reads

$$\ddot{x} + \alpha |\dot{x}|\, \dot{x} + x - x^3 = 0. \tag{106}$$

The nonescaping region is the basin of attraction of $(0, 0)$, and its boundary in the $(x, \dot{x})$ plane is the union of the stable manifolds of the two saddles $(\pm 1, 0)$.

5.1 Branchwise *p*-equation and explicit primitives

On each monotone branch with fixed velocity sign $\sigma \in \{+1, -1\}$, the reduction $p(x) = \dot{x}^2$ yields

$$\frac{\mathrm{d}p}{\mathrm{d}x} + 2\alpha\sigma\, p = -2V'(x) = -2x + 2x^3. \tag{107}$$

Introduce the primitives

$$\begin{aligned} I_\sigma(x) &:= \int^x (-2s + 2s^3)\, e^{2\alpha\sigma s}\, \mathrm{d}s, \\ p_\sigma(x; x_T) &= e^{-2\alpha\sigma x}\big[I_\sigma(x) - I_\sigma(x_T)\big], \end{aligned} \tag{108}$$

where x_T is a turning point (in particular, a saddle can be used as x_T because $p(x_T) = 0$ there).

For a constant α, one convenient closed form is

$$I_+(x) = e^{2\alpha x}\, \frac{4\alpha^3 x^3 - 4\alpha^3 x - 6\alpha^2 x^2 + 2\alpha^2 + 6\alpha x - 3}{4\alpha^4}, \tag{109}$$

$$I_-(x) = e^{-2\alpha x}\, \frac{-4\alpha^3 x^3 + 4\alpha^3 x - 6\alpha^2 x^2 + 2\alpha^2 - 6\alpha x - 3}{4\alpha^4}. \tag{110}$$

5.2 Saddle separatrices and the escape boundary

The basin boundary is obtained by launching from each saddle $(x_s, 0)$ with $p(x_s) = 0$ and following the two velocity branches $\sigma = \pm 1$. For each saddle, this produces an upper branch ($\dot{x} > 0$) and a lower branch ($\dot{x} < 0$).

Fig. 13 Quartic potential $V(x) = \frac{1}{2}x^2 - \frac{1}{4}x^4$ with a stable equilibrium at $x = 0$ and local maxima (barriers) at $x_s = \pm 1$

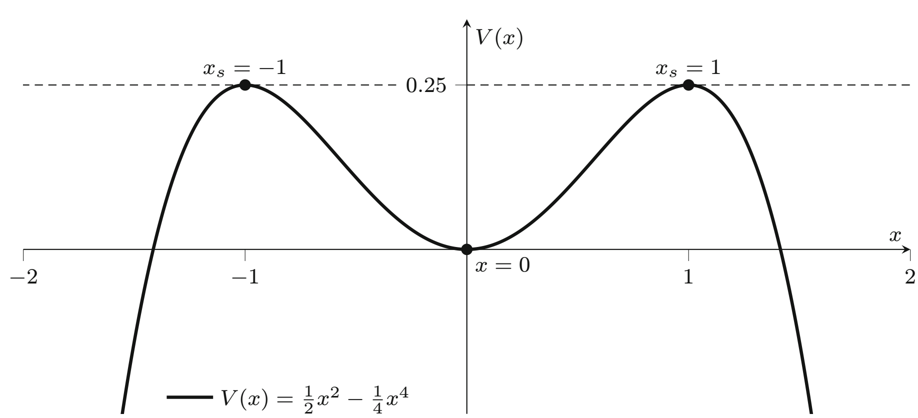

5.2.1 Right saddle $(1, 0)$

Setting $x_T = 1$ in Eq. (108) gives the two phase-plane graphs through $(1, 0)$,

$$p_+^{(1)}(x) := p_+(x; 1) = \frac{1}{4\alpha^4}\Big(4\alpha^3x^3 - 4\alpha^3x - 6\alpha^2x^2 + 2\alpha^2 + 6\alpha x - 3 + (4\alpha^2 - 6\alpha + 3)e^{2\alpha(1-x)}\Big), \tag{111}$$

$$p_-^{(1)}(x) := p_-(x; 1) = \frac{1}{4\alpha^4}\Big(- 4\alpha^3x^3 + 4\alpha^3x - 6\alpha^2x^2 + 2\alpha^2 - 6\alpha x - 3 + (4\alpha^2 + 6\alpha + 3)e^{2\alpha(x-1)}\Big). \tag{112}$$

The corresponding separatrix branches are

$$\dot{x} = +\sqrt{p_+^{(1)}(x)} \quad \text{(upper)}, \qquad \dot{x} = -\sqrt{p_-^{(1)}(x)} \quad \text{(lower)}, \tag{113}$$

restricted to the admissible set where the square root is real.

5.2.2 Left saddle $(-1, 0)$

Similarly, setting $x_T = -1$ yields the branches through $(-1, 0)$,

$$p_+^{(-1)}(x) := p_+(x; -1) = \frac{1}{4\alpha^4}\Big(4\alpha^3x^3 - 4\alpha^3x - 6\alpha^2x^2 + 2\alpha^2 + 6\alpha x - 3 + (4\alpha^2 + 6\alpha + 3)e^{-2\alpha(x+1)}\Big), \tag{114}$$

$$p_-^{(-1)}(x) := p_-(x; -1) = \frac{1}{4\alpha^4}\Big(- 4\alpha^3x^3 + 4\alpha^3x - 6\alpha^2x^2 + 2\alpha^2 - 6\alpha x - 3 + (4\alpha^2 - 6\alpha + 3)e^{2\alpha(x+1)}\Big). \tag{115}$$

By symmetry of Eq. (106) under $(x, \dot{x}) \mapsto (-x, -\dot{x})$, these curves are mirror images of the $(1, 0)$ separatrix.

5.2.3 Escape versus nonescape

The basin boundary (separatrix set) is

$$\mathcal{S}(\alpha) = \Big\{(x, \dot{x}) : \dot{x} = \pm\sqrt{p_\pm^{(1)}(x)}\Big\} \cup \Big\{(x, \dot{x}) : \dot{x} = \pm\sqrt{p_\pm^{(-1)}(x)}\Big\}, \tag{116}$$

interpreted branchwise with the admissibility restriction $p \geq 0$. Initial conditions inside the region enclosed by $\mathcal{S}(\alpha)$ are attracted to $(0, 0)$, while initial conditions outside cross one of the barriers and then escape to $\pm\infty$. A graphical example for $\alpha = 0.2$ is given in Fig. 14.

5.3 Local integrity measure with respect to $(0, 0)$

We define the local integrity measure about the stable equilibrium as

$$r_{\text{loc}}(\alpha) := \min_{(x,\dot{x})\in\mathcal{S}(\alpha)} \sqrt{x^2 + \dot{x}^2}. \tag{117}$$

By symmetry, it is sufficient to minimize the squared radius on the upper branch from the right saddle,

$$r^2(x; \alpha) = x^2 + p_+^{(1)}(x), \quad x \text{ in the admissible interior segment between 0 and 1.} \tag{118}$$

5.3.1 Interior tangency condition

An interior minimizer satisfies $\frac{\mathrm{d}}{\mathrm{d}x} r^2(x; \alpha) = 0$. Using Eq. (107) with $\sigma = +1$ gives

$$\begin{aligned}\frac{\mathrm{d}}{\mathrm{d}x} r^2(x; \alpha) &= 2x + p_+'(x; 1)\\ &= 2x + \big(-2\alpha\, p_+(x; 1) - 2x + 2x^3\big)\\ &= 2\big(x^3 - \alpha\, p_+(x; 1)\big),\end{aligned} \tag{119}$$

hence, the tangency relation

$$\alpha\, p_+^{(1)}(x_*) = x_*^3. \tag{120}$$

At such a point,

$$r_{\text{int}}^2(\alpha) = x_*^2 + p_+^{(1)}(x_*) = x_*^2 + \frac{x_*^3}{\alpha}, \qquad r_{\text{int}}(\alpha) = \sqrt{r_{\text{int}}^2(\alpha)}. \tag{121}$$

The potential-specific conversion of this tangency equation to a generalized Lambert form is given in Appendix B. Inserting the resulting tangency point from Eq. (141) into Eq. (121) gives $r_{\text{int}}(\alpha)$ explicitly.

5.3.2 Endpoint candidate and final *LIM* expression

The saddles $(\pm 1, 0)$ belong to the separatrix, giving the endpoint radius $r_{\text{end}} = 1$. Therefore, the local integrity measure is obtained as the lower envelope

$$r_{\text{loc}}(\alpha) = \min\big\{\, 1,\ r_{\text{int}}(\alpha)\,\big\}, \tag{122}$$

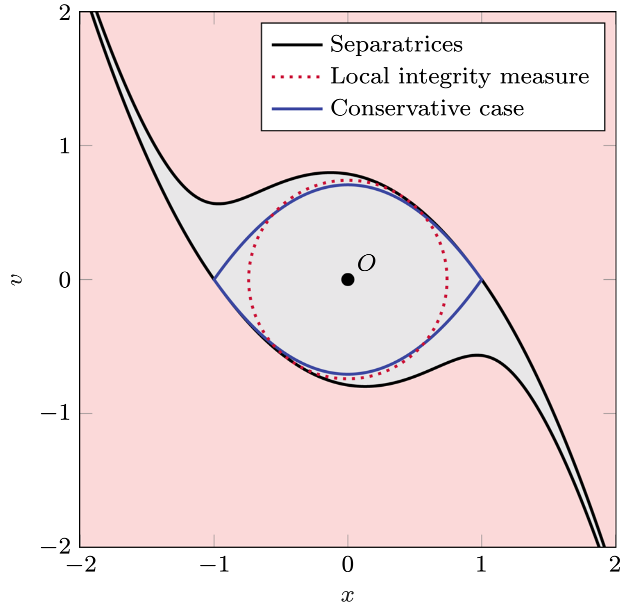

Fig. 14 Verification of the analytically determined basin-of-attraction boundary against numerical simulation data for $\alpha = 0.2$

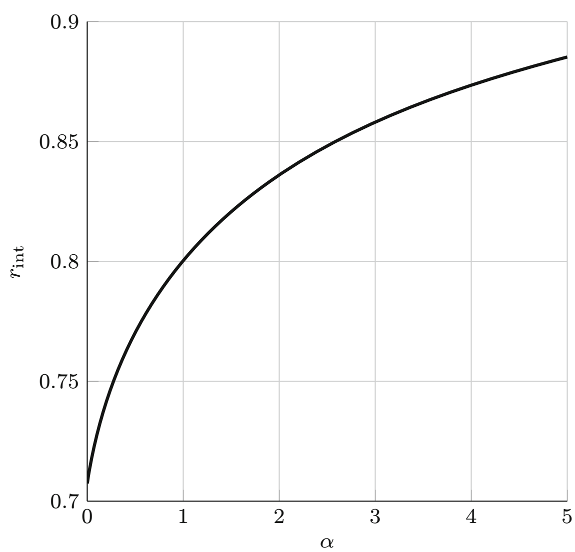

Fig. 15 Local integrity measure as a function of α for the quadratic–quartic Duffing potential

with $r_{\mathrm{int}}(\alpha)$ given by Eqs. (121) and (141). The *LIM* is plotted for $\alpha \in [0, 5]$ in Fig. 15.

6 Conclusions

This paper provides a constructive description of basin-of-attraction boundaries for autonomous one-degree-of-freedom systems with quadratic air drag. The central step is the branchwise reduction $p(x) = \dot{x}^2$, which yields a first-order equation that can be evaluated explicitly for several representative potentials and used to assemble the stable-manifold branches emanating from saddles. This yields sharp threshold criteria for escape versus capture, as well as closed-form expressions for the basin boundary and local integrity measures. The resulting expressions are suitable both for parameter studies and as reference cases for validating numerical basin computations.

Although the examples in this paper mainly use the air-drag coefficient as the varying parameter, the analytical formulas are useful beyond isolated numerical case studies. Once a formula for a basin boundary or a local integrity measure is available, whole parameter intervals can be evaluated without recomputing stable manifolds by time integration for many selected parameter values. The advantage becomes larger for systems with additional control parameters, provided that the same branchwise construction can be applied after the relevant saddle-type roots have been identified. The formulas are also useful for determining exact regime boundaries in the local integrity measure. Numerical optimization or dense sampling can approximate these curves, but the analytical treatment directly identifies the parameter ranges and possible non-smooth or discontinuous changes, as seen in the examples in Sects. 3 and 4.

The construction also clarifies how changes to parameters affect safe basins. Since the quadratic drag term vanishes at rest, the equilibrium positions are determined by the roots of $F(x; \mathbf{c}) = V_x(x; \mathbf{c})$, where $\mathbf{c}$ denotes control parameters. For positive drag, minima of the potential act as attractors, whereas maxima form saddle-type barriers whose stable manifolds bound the safe basins. Therefore, qualitative changes in the basin structure occur when the root structure of F changes, namely at nonhyperbolic equilibria satisfying $F = 0$ and $F_x = 0$.

The methodology used in the preceding sections extends directly to such parameter-dependent cases. After the relevant saddle-type roots have been identified, the same branchwise integral representation from Sect. 2 can be started at these saddles and continued through the admissible intervals, with branch switches at turning points. Thus, the local bifurcation determines which equilibria and saddle branches exist, while the global continuation of those branches determines the actual basin boundary.

For a smooth one-parameter path, the generic local event is a fold or saddle-node of critical points, where a minimum and a neighboring maximum are created or annihilated together. The local distance from the newly created attractor to the adjacent saddle-type barrier tends to zero at the bifurcation, so the local integrity measure of that attractor tends to zero. This is not, however, a statement about the global integrity measure based on total phase-space measure: a basin may have an arbitrarily narrow channel extending to infinity, and such an unbounded tail can make the global measure infinite even when the local distance to the boundary is small.

Transcritical and pitchfork bifurcations rearrange existing basin geometry rather than simply creating a new local minimum–maximum pair. In a transcritical bifurcation, two equilibrium branches exchange attracting and saddle-type roles. In a pitchfork bifurcation, one basin can split into two basins separated by a newly formed saddle-type branch, or merge again in the reverse crossing. With two or more control parameters, cusp-type degeneracies organize fold events and change the associated safe basins through the same saddle-branch continuation.

7 Scope for future research

The framework naturally accommodates the inclusion of additional non-smooth dissipation mechanisms, in particular, Coulomb friction, leading to the generalized equation of motion

$$\begin{aligned} &\ddot{x} + \alpha(x)\,|\dot{x}|\,\dot{x} + \beta(x)\ \mathrm{sgn}(\dot{x}) + V'(x) = 0, \\ &\quad \alpha(x) \geq 0,\ \ \beta(x) \geq 0, \end{aligned} \tag{123}$$

where $\alpha(x)$ and $\beta(x)$ denote spatially varying air-drag and dry-friction coefficients, respectively. Since both air drag and Coulomb friction introduce discontinuities through $|\dot{x}|$ and $\mathrm{sgn}(\dot{x})$, the setting is naturally linked to classical dry-friction models and to differential equations with discontinuous right-hand side [57–59]. At $\dot{x} = 0$, the Coulomb term is discontinuous and is naturally interpreted in the Filippov sense as the set-valued force $\beta(x)\,\mathrm{sgn}(\dot{x}) \in [-\beta(x), +\beta(x)]$. This admits *sticking* intervals: if at some position x_s one has $|V'(x_s)| \leq \beta(x_s)$, then friction can balance the conservative force, and $\dot{x}$ may remain zero. In that case, the dynamics terminate (capture) at x_s rather than continuing with a branch switch. If instead $|V'(x_s)| > \beta(x_s)$, the motion must leave $\dot{x} = 0$, and the subsequent evolution proceeds on the appropriate sliding branch.

For multi-degree-of-freedom systems, the present reduction does not extend to a generic phase space without additional structure. The clearest possible extension occurs when the dynamics contain an effectively one-dimensional invariant subsystem. Consider, for example, the two-degree-of-freedom model

$$\ddot{\mathbf{q}} + \alpha(\mathbf{q})\,\|\dot{\mathbf{q}}\|\,\dot{\mathbf{q}} + \nabla V(\mathbf{q}) = 0$$

and a smooth arclength-parametrized curve $\Gamma : \mathbf{q} = \gamma(s)$ with tangent $\tau(s) = \gamma'(s)$. For a trajectory lying on this curve, $\mathbf{q}(t) = \gamma(s(t))$, one has

$$\dot{\mathbf{q}} = \tau\,\dot{s}, \qquad \ddot{\mathbf{q}} = \tau\,\ddot{s} + \gamma''(s)\dot{s}^2, \qquad \|\dot{\mathbf{q}}\| = |\dot{s}|.$$

After substitution into the two-degree-of-freedom equation, the tangent part is obtained by multiplying with τ^T, while the normal part is obtained by applying the projector $I - \tau\tau^T$. Since γ is arclength-parametrized, $\tau^T\gamma'' = 0$, and one obtains the tangential equation and the normal compatibility condition

$$\begin{aligned} &\ddot{s} + \alpha(\gamma(s))\,|\dot{s}|\,\dot{s} + \frac{d}{ds}V(\gamma(s)) = 0, \\ &(I - \tau\tau^T)\nabla V(\gamma(s)) + p(s)\gamma''(s) = 0, \end{aligned}$$

where $p(s) = \dot{s}^2$. On each velocity branch $\sigma = \mathrm{sgn}(\dot{s})$, the tangential equation has the same form as in the one-degree-of-freedom case:

$$p'(s) + 2\sigma\,\alpha(\gamma(s))\,p(s) = -2\,\frac{d}{ds}V(\gamma(s)).$$

The second condition is the additional restriction absent in one degree of freedom. It is necessary because, otherwise, an initial condition tangent to Γ acquires a normal acceleration that is not the geometric normal acceleration of the curve and therefore immediately leaves Γ. If a whole tangent bundle over Γ is to be invariant, namely if arbitrary tangent initial velocities should remain on the curve, this normal condition must hold for all p. In the unconstrained isotropic model above, this is possible only in the straight invariant case $\gamma'' = 0$ together with $(I - \tau\tau^T)\nabla V(\gamma(s)) = 0$. Thus, a symmetry line, for example, $y = 0$ with $V_y(x, 0) = 0$, yields a genuine two-degree-of-freedom system that is reducible by the present method. For a curved path, the normal equation can at most hold for a particular branch speed $p(s)$, which must then satisfy both the normal compatibility condition and the scalar branch equation. Generic two-degree-of-freedom stable manifolds are higher-dimensional subsets of the four-dimensional phase space and remain outside the scope of the present paper. Identifying which physically relevant multi-degree-of-freedom systems satisfy such invariant-curve conditions is therefore an open question for future research.

Further relevant extensions to the current study are: (i) periodic and tilted periodic pendulum-related potentials, where the outcome classes include rotation and transport across multiple wells; (ii) infinite potentials, such as the Pöschl–Teller potential [60], central-field models with quadratic drag [11], and the Morse potential [61]; (iii) spatially varying drag and friction laws, where the branchwise construction remains valid but typically requires quadrature and careful handling of sticking; (iv) extension to systems with non-quadratic damping, such as $\sim \alpha\,\mathrm{sgn}(\dot{x})|\dot{x}|^{\gamma}$, where the reduction $p(x) = \dot{x}^2$ can still yield an analytically solvable, non-linear first-order differential equation; (v) classifying further multi-degree-of-freedom systems with invariant one-dimensional reductions or other special structures that yield tractable reduced equations.

A Small-drag expansions

This appendix collects perturbation calculations useful for asymptotic checks but not required for the main basin-boundary construction.

A.1 Quadratic-cubic left turning point

For $0<\alpha<1$, the $\sigma=+1$ saddle branch of the quadratic-cubic potential possesses a finite left turning point $x_L(\alpha)<0$ determined by $p_+(x_L;1)=0$, equivalently by Eq. (30). Introduce

$$F(\alpha,x):=e^{2\alpha x}\Big(2\alpha^2x^2-2\alpha^2x-2\alpha x+\alpha+1\Big) -e^{2\alpha}(1-\alpha), \tag{124}$$

so that $x_L(\alpha)$ is defined by $F(\alpha,x_L(\alpha))=0$. Expanding for fixed x gives

$$F(\alpha,x)=\alpha^3\Big(\frac{4}{3}x^3-2x^2+\frac{2}{3}\Big)+\alpha^4\Big(2x^4-\frac{8}{3}x^3+\frac{2}{3}\Big) +\alpha^5\Big(\frac{8}{5}x^5-2x^4+\frac{2}{5}\Big)+\mathcal{O}(\alpha^6). \tag{125}$$

With

$$x_L(\alpha)=x_0+x_1\alpha+x_2\alpha^2+\mathcal{O}(\alpha^3), \qquad \alpha\to 0^+, \tag{126}$$

substitution into $F(\alpha,x_L(\alpha))=0$ yields

$$F(\alpha,x_L(\alpha))=\alpha^3C_3+\alpha^4C_4+\alpha^5C_5+\mathcal{O}(\alpha^6)=0, \tag{127}$$

where

$$C_3=\frac{4}{3}x_0^3-2x_0^2+\frac{2}{3}, \tag{128}$$

$$C_4=2x_0^4-\frac{8}{3}x_0^3+4x_0^2x_1-4x_0x_1+\frac{2}{3}, \tag{129}$$

$$C_5=\frac{8}{5}x_0^5-2x_0^4+8x_0^3x_1-8x_0^2x_1+4x_0^2x_2+4x_0x_1^2 -4x_0x_2-2x_1^2+\frac{2}{5}. \tag{130}$$

Solving $C_3=C_4=C_5=0$ and selecting the left turning point gives

$$x_L(\alpha)=-\frac{1}{2}-\frac{3}{8}\alpha-\frac{21}{80}\alpha^2+\mathcal{O}(\alpha^3), \qquad \alpha\to 0^+. \tag{131}$$

A.2 Duffing endpoint candidate

For the upper left branch of the Duffing separatrix leaving the saddle $(0,0)$,

$$p_+(x;0)=e^{-2\alpha x}\int_0^x(2s-2s^3)e^{2\alpha s}\,ds. \tag{132}$$

The left turning point $x_L(\alpha)<0$ is characterized by

$$\int_0^{x_L(\alpha)}(2s-2s^3)e^{2\alpha s}\,ds=0. \tag{133}$$

Using $e^{2\alpha s}=1+2\alpha s+2\alpha^2s^2+\mathcal{O}(\alpha^3)$ gives

$$0=\Big(x_L^2-\tfrac{1}{2}x_L^4\Big)+\alpha\Big(\tfrac{4}{3}x_L^3-\tfrac{4}{5}x_L^5\Big) +\alpha^2\Big(x_L^4-\tfrac{2}{3}x_L^6\Big)+\mathcal{O}(\alpha^3). \tag{134}$$

Setting

$$x_L(\alpha)=-\sqrt{2}+a_1\alpha+a_2\alpha^2+\mathcal{O}(\alpha^3) \tag{135}$$

and matching powers of α yields $a_1=-4/15$ and $a_2=-\sqrt{2}/9$. Hence

$$x_L(\alpha)=-\sqrt{2}-\frac{4}{15}\alpha-\frac{\sqrt{2}}{9}\alpha^2+\mathcal{O}(\alpha^3), \quad \alpha\to 0^+, \tag{136}$$

and therefore

$$r_{\mathrm{end}}(\alpha)=|x_L(\alpha)+1| =(\sqrt{2}-1)+\frac{4}{15}\alpha+\frac{\sqrt{2}}{9}\alpha^2+\mathcal{O}(\alpha^3). \tag{137}$$

B Quadratic-quartic tangency equation

For the quadratic-quartic potential, substituting Eq. (111) into the tangency relation (120) and introducing $u:=2\alpha x$ yields

$$\Big(\frac{3}{2}u^2+(2\alpha^2-3)u+(3-2\alpha^2)\Big)e^u=(4\alpha^2-6\alpha+3)e^{2\alpha}. \tag{138}$$

Let

$$\widetilde{Q}(u;\alpha):=u^2+\frac{2(2\alpha^2-3)}{3}u+\frac{2(3-2\alpha^2)}{3} =(u-a_1(\alpha))(u-a_2(\alpha)), \tag{139}$$

where $a_{1,2}(\alpha)$ are the two roots of $\widetilde{Q}$. Then Eq. (138) becomes

$$(u-a_1(\alpha))(u-a_2(\alpha))e^u=\frac{2}{3}(4\alpha^2-6\alpha+3)e^{2\alpha}. \tag{140}$$

Using the generalized Lambert inverse $W(\cdot; a_1, a_2)$ [55, 56], the tangency location can be written as

$$u_*(\alpha) = W\left(\frac{2}{3}(4\alpha^2 - 6\alpha + 3)e^{2\alpha};\ a_1(\alpha), a_2(\alpha)\right),$$
$$x_*(\alpha) = \frac{u_*(\alpha)}{2\alpha}. \tag{141}$$

The physically relevant real branch is selected by the admissibility constraint $x_*(\alpha) \in (0, 1)$.

Acknowledgements We acknowledge the assistance of the following AI tools: OpenAI's ChatGPT, Grammarly, and Writefull.

Author Contributions All authors contributed to the paper's core idea. A.G. wrote the main manuscript text and prepared the figures. All authors reviewed the manuscript.

Funding Open Access funding enabled and organized by Projekt DEAL. This research was funded by the Deutsche Forschungsgemeinschaft (DFG, German Research Foundation) under Project Number 508244284 and by the Israel Science Foundation (grant 3085/25). We are sincerely grateful for their support.

Data availability No datasets were generated or analysed during the current study.

Declarations

Conflict of interest The authors declare no conflict of interest.

References

1. Dalzell, J.F.: A note on the form of ship roll damping. J. Ship Res. **22**, 178–185 (1978)
2. Cardo, A., Francescutto, A., Nabergoj, R.: On damping models in free and forced rolling motion. Ocean Eng. **9**, 171–179 (1982)
3. Bass, D.W., Haddara, M.R.: Nonlinear models of ship roll damping. Int. Shipbuild. Prog. **35**(401), 5–24 (1988)
4. Neves, M.A.S., Pérez, N.A., Valerio, L.: Stability of small fishing vessels in longitudinal waves. Ocean Eng. **26**, 1389–1419 (1999)
5. Taylan, M.: The effect of nonlinear damping and restoring in ship rolling. Ocean Eng. **27**, 921–932 (2000)
6. Simmonds, D.S.: The response of a simple pendulum with Newtonian damping. J. Sound Vib. **84**(3), 453–461 (1982)
7. Mungan, C.E., Lipscombe, T.C.: Oscillations of a quadratically damped pendulum. Eur. J. Phys. **34**(5), 1243–1253 (2013)
8. Morison, J.R., O'Brien, M.P., Johnson, J.W., Schaaf, S.A.: The force exerted by surface waves on piles. J. Petrol. Technol. **2**(5), 149–154 (1950)
9. Sarpkaya, T.: Wave Forces on Offshore Structures. Cambridge University Press, Cambridge (2010)
10. Fossen, T.I.: Handbook of Marine Craft Hydrodynamics and Motion Control. Wiley, Chichester (2011)
11. Humi, M., Carter, T.: Models of motion in a central force field with quadratic drag. Celest. Mech. Dyn. Astron. **84**, 245–262 (2002)
12. Knacke, T.W.: Parachute Recovery Systems: Design Manual. Para Pub, Santa Barbara, CA (1992)
13. Hoerner, S.F.: Fluid-Dynamic Drag: Practical Information on Aerodynamic Drag and Hydrodynamic Resistance. Hoerner Fluid Dynamics (1965)
14. Briggs, L.J.: Effect of spin and speed on the lateral deflection (curve) of a baseball; and the Magnus effect for smooth spheres. Am. J. Phys. **27**(8), 589–596 (1959)
15. Nathan, A.M.: The effect of spin on the flight of a baseball. Am. J. Phys. **76**(2), 119–124 (2008)
16. Alam, F., Ho, H., Smith, L., Subic, A., Chowdhury, H., Kumar, A.: A study of baseball and softball aerodynamics. Procedia Eng. **34**, 86–91 (2012)
17. Wylie, C.R., Jr.: Simple harmonic motion with quadratic damping. Am. Math. Mon. **47**, 474–476 (1940)
18. Klotter, K.: Free oscillations of systems having quadratic damping and arbitrary restoring forces. J. Appl. Mech. **22**, 493–499 (1955)
19. Richardson, P.D.: Free oscillations with damping proportional to the square of the velocity. Appl. Sci. Res. Sect. A **11**, 397–400 (1963)
20. Wittenburg, J.: Schwingungslehre. Springer-Lehrbuch, 1st edn. Springer, Berlin (1996)
21. Bogoliubov, N.N., Mitropolskii, Y.A.: Asymptotic Methods in the Theory of Nonlinear Oscillations. Gordon and Breach, New York (1961)
22. Andronov, A.A., Vitt, A.A., Khaikin, S.E.: Theory of Oscillators. Pergamon Press, Oxford (1966)
23. Nayfeh, A.H., Mook, D.T.: Nonlinear Oscillations. Wiley, New York (1979)
24. Cvetičanin, L.: Oscillator with strong quadratic damping force. Publications de l'Institut Mathématique (Beograd) (N.S.) **85**(99), 119–130 (2009)
25. Kovacic, I., Rakaric, Z.: Study of oscillators with a non-negative real-power restoring force and quadratic damping. Nonlinear Dyn. **64**, 293–304 (2011)
26. Rakaric, Z., Kovacic, I.: Energy analysis of Duffing oscillators with quadratic damping: exact solutions. J. Phys. Conf. Ser. **2090**, 012008 (2021)
27. Chiellini, A.: Sull'integrazione dell'equazione differenziale $y' + p(x)y + q(x)y^n = 0$. Bollettino dell'Unione Matematica Italiana **10**, 301–307 (1931)
28. Pandey, A., Ghose-Choudhury, A., Guha, P.: Chiellini integrability and quadratically damped oscillators. Int. J. Non-Linear Mech. **92**, 153–159 (2017)
29. Takahashi, D.A.: Newton's equation of motion with quadratic drag force and Toda's potential as a solvable one. Phys. Scr. **93**, 075204 (2018)
30. Newton, I.: Philosophiæ Naturalis Principia Mathematica, 1st edn. S. Pepys, London (1687)
31. Bernoulli, J.: Responsio ad nonneminis provocationem, tam de problemate, quod in actis eruditorum proposuit, quam de inventione lineae curvae, quam describit projectum in medio resistente. Acta Eruditorum, pp. 216–226 (1719). Maji (May) issue
32. Euler, L.: Neue Grundsätze der Artillerie, ins besondere in Ansehung des Widerstands der Luft nebst einem Anhange von den Eigenschaften des Pulvers, und den Wirkungen des Schießpulvers.

A. Haude, Berlin, 1745. German translation (with additions) of Benjamin Robins' New Principles of Gunnery
33. Lambert, J.H.: Von der bewegung der körper in widerstehenden mitteln. In *Beyträge zum Gebrauche der Mathematik und deren Anwendung*, vol. 3, pp. 102–188. Haude und Spener, Berlin (1767)
34. Borda, J.-C.: Mémoire sur le mouvement des projectiles. In: Histoire de l'Académie Royale des Sciences, pp. 116–121. Imprimerie Royale, Paris (1772)
35. Legendre, A.-M.: Dissertation sur la question de balistique proposée par l'Académie Royale des Sciences. Decker, Berlin (1782)
36. Didion, I.: Traité de balistique, 2nd edn. Mallet-Bachelier, Paris (1860)
37. Lamb, H.: Dynamics, 2nd edn. Cambridge University Press, London (1923)
38. Hackborn, W.W.: Projectile motion: Resistance is fertile. Am. Math. Mon. **115**(9), 813–819 (2008)
39. Hackborn, W.W.: On motion in a resisting medium: a historical perspective. Am. J. Phys. **84**(2), 127–134 (2016)
40. Ray, S., Fröhlich, J.: An analytic solution to the equations of the motion of a point mass with quadratic resistance and generalizations. Arch. Appl. Mech. **85**, 395–414 (2015)
41. Yabushita, K., Yamashita, M., Tsuboi, K.: An analytic solution of projectile motion with the quadratic resistance law using the homotopy analysis method. J. Phys. A: Math. Theor. **40**(29), 8403–8416 (2007)
42. Parker, G.W.: Projectile motion with air resistance quadratic in the speed. Am. J. Phys. **45**(7), 606–610 (1977)
43. Tsuboi, N.: On the optimum angle of takeoff in long jump. Trans. Jpn. Soc. Ind. Appl. Math. **6**, 393 (1996)
44. Soliman, M.S., Thompson, J.M.T.: The effect of damping on the steady state and basin bifurcation patterns of a nonlinear mechanical oscillator. Int. J. Bifurc. Chaos **2**(1), 81–91 (1992)
45. Zhong, J., Ross, S.D.: Geometry of escape and transition dynamics in the presence of dissipative and gyroscopic forces in two degree of freedom systems. Commun. Nonlinear Sci. Numer. Simul. **82**, 105033 (2020)
46. Margheri, A., Misquero, M.: A dissipative Kepler problem with a family of singular drags. Celest. Mech. Dyn. Astron. **132**(3), 17 (2020)
47. Soliman, M.S., Thompson, J.M.T.: Integrity measures quantifying the erosion of smooth and fractal basins of attraction. J. Sound Vib. **135**(3), 453–475 (1989)
48. Soliman, M.S., Thompson, J.M.T.: Stochastic penetration of smooth and fractal basin boundaries under noise excitation. Dyn. Stab. Syst. **5**(4), 281–298 (1990)
49. Lenci, S., Rega, G., Ruzziconi, L.: The dynamical integrity concept for interpreting/predicting experimental behaviour: from macro- to nano-mechanics. Philos. Trans. R. Soc. A Math. Phys. Eng. Sci. **371**(1993), 20120423 (2013)
50. Rega, G., Lenci, S.: Identifying, evaluating, and controlling dynamical integrity measures in non-linear mechanical oscillators. Nonlinear Anal. Theory Methods Appl. **63**(5–7), 902–914 (2005)
51. Leszczyński, M., Perlikowski, P., Burzyński, T., Kowalski, T.M., Brzeski, P.: Review of sample-based methods used in an analysis of multistable dynamical systems. Chaos **32**(8), 082101 (2022)
52. Habib, G.: Dynamical integrity assessment of stable equilibria: a new rapid iterative procedure. Nonlinear Dyn. **106**, 2073–2096 (2021)
53. Patkó, D., Habib, G.: Dynamical integrity of periodic orbits: a computationally efficient approach. Nonlinear Dyn. **113**, 24641–24661 (2025)
54. Kravetc, P., Gendelman, O., Fidlin, A.: Dynamical integrity of the safe basins in a problem of forced escape. Chaos **34**(8), 083118 (2024)
55. Mező, I., Baricz, Á.: On the generalization of the Lambert W function with applications in theoretical physics. arXiv:1408.3999 (2015)
56. Mező, I., Baricz, Á.: On the generalization of the Lambert W function. Trans. Am. Math. Soc. **369**(11), 7917–7934 (2017)
57. Den Hartog, J.P.: Mechanical Vibrations. McGraw-Hill, New York (1934)
58. Filippov, A.F.: Differential Equations with Discontinuous Righthand Sides. Kluwer Academic, Dordrecht (1988)
59. Fay, T.H.: Quadratic damping. Int. J. Math. Educ. Sci. Technol. **43**(6), 789–803 (2012)
60. Pöschl, T.: Zur Frage der Schwingungen nach dem quadratischen Widerstandskraftgesetz. Physikalische Zeitschrift **29**, 938 (1928)
61. Morse, P.M.: Diatomic molecules according to the wave mechanics. II. Vibrational levels. Phys. Rev. **34**, 57–64 (1929)